Mario E. Cordero[1,2] / Sebastián Uribe[1] / Luis G. Zárate[1] / Jose A. Hernandez-Servin[3] / Ever Peralta Reyes[4] / Alejandro Regalado-Méndez[4] / Reyna Natividad[2]

CFD Analysis of BED Textural Characteristics on TBR Behavior: Hydrodynamics and Scaling-up

[1] Departamento de Ingenierías, Escuela de Ingeniería Química, Universidad Popular Autónoma del Estado de Puebla, México, 21 Sur, Barrio de Santiago, C.P. 72410 Puebla, México, E-mail: marioedgar.cordero@upaep.mx
[2] Centro Conjunto de Investigación en Química Sustentable UAEM-UNAM, Carretera Toluca-Atlacomulco Km 14.5, Toluca Estado de México 50200, México, E-mail: marioedgar.cordero@upaep.mx
[3] División de Computación, Facultad de Ingeniería, Universidad Autónoma del Estado de México, Cerro de Coatepec, Toluca, Edo. De México, México
[4] Universidad del Mar, Ciudad Universitaria s/n, Puerto Ángel, Distrito de San Pedro Pochutla, C.P. 70902 Oaxaca, México. http://orcid.org/0000-0002-5270-745X.

Abstract:
In recent years, CFD has played an important role in the understanding and design of TBR's. In this work, through CFD with Eulerian approach, a three-phase heterogeneous reactor model was developed, were the accuracy of Interfacial Momentum Exchange Model (IMEM) for the gas-solid interaction, the effect of a more detailed catalytic bed geometry description, and the pellet shape over TBR hydrodynamics of two fluid phases interacting with the solid phase was studied. Then, a second model was developed, where the validated hydrodynamic model was coupled with mass transport for an HDS process of light gasoil. Additionally, in order to insight into the scaling up process of a TBRs, the proposed columns behaviors were compared against literature columns using four different ways, and it was found that the best predictions were obtained when the models' holdup were equaled to those evaluated in literature columns. Since in reliable literature deviations in pressure drop predictions of around 30% can be found, the model results show significant improvement against literature, achieving 5 times better accuracy in predicting pressure drops, and 50% improvement in holdup prediction; the coupled model reproduces the same conversion values compared with literature data, and predicts conversions with 95% accuracy

Keywords: TBR CFD simulation, catalyst geometry, bed porosity, scale-up process, hydrodesulphurization

DOI: 10.1515/ijcre-2017-0095

Received: June 5, 2017; **Accepted:** September 14, 2017

1 Introduction

Trickle Bed Reactors (TBR) are widely used in several industries such as hydrotreating, wastewater treatment, and in other applications such as biochemical processing (Wei et al. 2017; Gunjal and Ranade 2007). Furthermore, due to their large production volumes, there is an economic incentive to improve TBR performance (Malang, Kumar, and Saptoro 2015; Dudukovic 2007). In the TBR design, scale-up and optimization, complex interactions between hydrodynamics, mass transfer and reaction phenomena represent an almost insurmountable obstacle (Liu et al. 2009). Despite this difficulty, through many experimental and theoretical works, it has been identified that the design, scale up and optimization demand a reliable evaluation of hydrodynamic key parameters like holdup and pressure drop (Nadeem, Salem, and Sassi 2017; Al-Dahhan and Dudukovic 1995; Iliuta, Larachi, and Grandjean 1988; Atta, Roy, and Nigam 2007; Lasseux and Valdés-Parada 2017; Al-Dahhan and Dudukovic 1994; Ellman et al. 1990; Jindal and Buwa 2016), wet efficiency and regime transition (Bandari, Behjat, and Shahhosseini 2012; Solomenko et al. 2015; Kundu, Nigam, and Verma 2003). In addition, the inherent problem of liquid mal-distribution, that reduces the conversion, has to be taken into account for the TBR performance improvement (Solomenko et al. 2015). However, due to the highly coupled nature, multivariable and multiscale of these systems, there is no theory that fully explains such systems (Kundu, Nigam, and Verma 2003). In this sense, phenomenological models have been proposed in order to predict TBR's hydrodynamic parameters. These models, however, are mostly characterized for being based on idealization of the pore space (Lasseux and Valdés-Parada 2017; Mitra 2011). As an example of this, the Attou model considers a simplified

Mario E. Cordero is the corresponding author.

ordered and non-random geometrical model of porous interstitial space, that consists of few nonrandom pellets where an annular flow of liquid is established, which perfectly wets the solid and noncontact gas and solid phases, therefore there is no gas-solid interaction (Attou, Boyer, and Ferschneider 1999). Similar aspects can be pointed out in models based on the slit concept (Iliuta and Larachi 1999).

This kind of idealizations is what actually prevents the proper prediction of some observed phenomena that are ascribed to the inhomogeneity of the pore space of reactor bed. In fact, the use of these widely applied models in TBR's lead to acceptable holdup predictions with Mean Absolute Relative Error (MARE) barely above 10 %. Nevertheless, considerable deviations, of around 30 %, in estimating pressure drops at high pressure operation can also be observed (Iliuta, Larachi, and Grandjean 1988; Mitra 2011; Nadeem, Salem, and Sassi 2017). Thus, the current understanding and mathematical representation of hydrodynamics of these reactors is not satisfactory enough, and given the magnitude of the deviations in the predictions of these hydrodynamic parameters, it cannot be assumed that the analysis task is completed yet.

In some extent, the basic problem lies on the difficulties in measuring and describing both the very complex gas-liquid, gas-solid, and liquid-solid phase interactions and their coupled effect with the catalyst geometry that arises due to the size, shape and packing method of the bed particles (Ellman et al. 1990; Iliuta and Larachi 1999). These phenomena also prevent the existence of a robust methodology for scale up process of TBR's (Dudukovic 2009). Regarding studies that consider the effect of the geometry and size of the catalyst and the porosity of the bed, those of Al-Dahhan and Nemec (Al-Dahhan and Dudukovic 1994; Nemec and Levec 2005) can be highlighted, who experimentally determined pressure drop and holdup for systems at high pressures, in a wide range of particle size, bed porosities and operating conditions. They found that the pressure drop is highly sensitive to variations of the bed textural properties. Another observation that comes into view, since the operating pressure range is several orders of magnitude, is that the accuracy of prediction of the pressure drop is low. It has also been observed that the pellet shape has an important effect over the kinetics behavior (Carruthers and DiCamillo 1988; Afandizadeh and Foumeny 2001; Macias and Ancheyta 2004); and in addition, that considering form-factors, what is the usual way to take into account the geometrical features of the bed are not sufficient enough to get a good prediction (Trivizadakis, Giakoumakis, and Karabelas 2006; Bazmi, Hashemabadi, and Bayat 2013). Thus, further studies on the effect of the catalyst geometry considering more than just a form factor like the equivalent diameter or area to pellet volume ratio are desirable, this is, considering the textural bed characteristics as tortuosity and interstitial space geometry.

As an effort to provide more knowledge about the TBR behavior, Computer fluid dynamics (CFD) has emerged as an alternative, since it can provide important gain of time, reduces the number of experiments (Hu and Li 2007; Prasad et al. 2010) and allows to access information at the local scale phenomenon, that is generally not (or hardly) measurable with experimental methods. Also, CFD allows taking into account more realistic operating conditions (high temperature and pressure, reactive conditions, etc.) in the evaluation of hydrodynamics parameters in TBRs as pressure drop and liquid holdup than those evaluated experimentally in cold columns (Augier, Idoux, and Delenne 2010), without consideration of the chemical reaction.

In literature related to single and multiphase CFD simulations of TBRs two types of contributions may be distinguished: 1) works where the complex description of void volume are not rigorously taken into account to describe the interactions between phases, but its simplicity allows to incorporate complexities like chemical reactions into the modelling (Niegodajew, Asendrych, and Drobniak 2013; Horgue et al. 2013; Bazmi, Hashemabadi, and Bayat 2012); and 2) investigations where the size and shape of catalyst are taken into account to describe more explicitly the interstitial space between the bed particles. These studies have generally appealed to geometry simplifications as low reactor/pellet diameter ratios, or simplification in multiphysics nature thus only considering the study of the hydrodynamics or the hydrodynamics and heat transfer. Such studies incorporate turbulence, the effect of radial porosity, and couple the hydrodynamics of single phase with mass and energy equations (Derkx and Dixon 1996; Nijemeisland and Dixon 2001; Lopes and Quinta-Ferreira 2009; Lappalainen, Manninen, and Alopaeus 2009; Augier et al. 2010; Reddy and Joshi 2010; Beni and Khosravi-Nikou 2016)

In this sense, it is possible to find several reported works in literature addressed to the study of the coupled phenomena present in chemical reactors through CFD simulations. However, these works usually have strong emphasis in the hydrodynamics, such as the works of Quinta-Ferreira et al. (Lopes and Quinta-Ferreira 2010a; Lopes and Quinta-Ferreira 2010b) or Beni and Khosravi-Nikou work, which also involves the low ratio of reactor diameter to pellet diameter value $(N \simeq 3)$ (Beni and Khosravi-Nikou 2016).

The Mousazadeh et al., Parpatou et al. and Peng et al. (Peng et al. 2016) works (Mousazadeh, Van Den Akker, and Mudde 2013; Partopour and Dixon 2016; Peng et al. 2016) are recent efforts by coupling the hydrodynamics and the mass transport. However, they again involve low N values, and do not need to consider IMEMs as closures to model the interactions between fluid phases, as they consider two-phase reactors with a unique fluid phase. Due to the aforementioned, it can be seen that there is a lack of works with more realistic fluid dynamics representations and that consider the flow and concentrations heterogeneities between particles and

including reaction with different catalyst shape and sizes, and therefore more studies are required. In fact, this should be the main objective for the next decade to come (Partopour and Dixon 2016).

On the other hand, it is well known that there is no well-established scaling-up/down procedure for TBR's, and which in practice is based on equaling the Liquid Hourly Space Velocity (LHSV) (Dorai et al. 2015). However, this equality involves lower pilot plant velocities, from 10 to 100 times lower than industrial plants (Sie 1990), causing a counterproductive effect on the mass transfer resistances, and modifying the plug-flow behavior inside the reactor. Recently, the size reduction or down-scaling of pilot reactors has become a more important requirement and an important incentive for the development and improvement of scaling techniques; this issue represents one of the greatest challenges in the years to come. It is clear that a scale up/down process based on knowledge of the hydrodynamics of the reactor with more scientific bases is required, and that possessing a scale-up/down process with those characteristics could imply that development costs could be reduced because the amount of prototype catalyst and reactors to be tested would be reduced.

In this context, this work aims to study through CFD the effect of a more representative geometry of catalyst bed that incorporates more textural effects like the catalyst shape and size, over the improvement of hydrodynamics parameters prediction (pressure drop and liquid holdup) and over the kinetic and hydrodynamic behavior of a co-current TBR operating at Trickle regime that couple hydrodynamics and mass transport. The study of mass transport includes a HDS reaction that follows a LHHW kinetics found in literature (Chacón et al. 2012).

In order to explore a suitable reactor scaling-up procedure, a comparative study of two TBR's with different lengths and diameters was implemented, searching in which conditions a similar hydrodynamic and conversion values between both systems are obtained. For this purpose, both reactors were compared equaling the Reynolds numbers $\left(\mathrm{R}e_{\gamma} - \mathrm{R}e_{\beta}\right)$, the mass flow rates $(L - G)$, the holdups $\left(\varepsilon_{\gamma} - \varepsilon_{\beta}\right)$ and the hourly space velocities $(LHSV - GHSV)$.

2 Theory

2.1 Geometric packed bed models

A heterogeneous reactor model was developed in which both interstitial and catalytic bed domains were built by using 12 layers of pellets. The three first layers consisted of 60, 61, and 60 pellets respectively, then these three layers were repeated four times to complete the geometrical model, details are shown in Figure 1(a) and Figure 1(b). The complete TBR's geometrical model contained 724 spherical particles of 1.52 mm of diameter and had a bed porosity $(\varepsilon_B)$of 0.41, 0.48 and 0.49. For comparison purposes of pressure drop, these parameters were selected according to the experimental work of Al-Dahhan et al., (Al-Dahhan and Dudukovic 1994). Also, for validation purposes of kinetic behavior, a 0.35 mm pellet diameter and bed porosity of 0.41 were considered according to Chacon work (Chacón et al. 2012). It is known that to avoid wall effects, there is a critical value (N) of the reactor to pellet diameters ratio D_R/d_P that must be considered in modelling of this kind of systems. According to the aforementioned, a value of $N \approx 9.1$ for hydrodynamics simulations and $N \approx 18.4$ in simulations coupling mass transport seem to be adequate and, these values were selected based on CFD literature works (Bazmi, Hashemabadi, and Bayat 2012; Chacón et al. 2012; Guardo et al. 2006). It is worth noticing that in experimental works higher values can be found; for example, the value used by Al-Dahhan is $N = 14.1$ for his hydrodynamic analysis (Al-Dahhan and Dudukovic 1994).

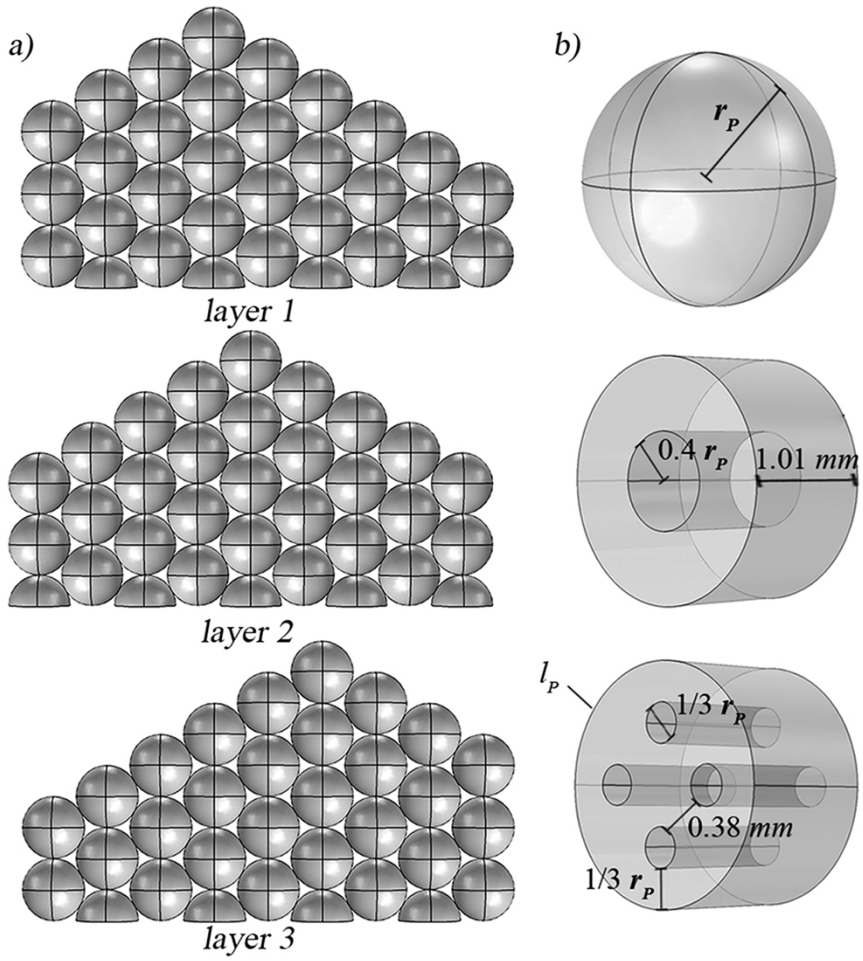

Figure 1: (a) Schematic representation of geometric relationship of first three layers of the bed, and (b) details of the construction spherical, RR and 4HC pellets geometries used.

Regarding to reactor configurations, two different configurations were implemented; a configuration for hydrodynamics (cold column) cases with $N \approx 9.1$, $d_P = 1.52$ mm, with Hexane and N_2 as liquid and gas fluids; and another completely different for HDS reactor case with $N \approx 18.4$, $d_P = 0.35$ mm, with gasoil and H_2 as liquid and gas fluids.

Figure 1(b) shows some of the construction details of the catalysts used in this study. The distances between pellets and reactor wall and between adjacent pellets (DIS) were adjusted for each pellet shape to satisfy the selected bed void fraction and both type of particles, the Raschig rings (RR) and cylinders with four longitudinal holes$(4HC)$, have the same relative cross-sectional area/volume (S_T/V_P) of catalyst than the spheres. More details about the different catalyst geometries assessed in this work, are shown in Table 1.

Table 1: Geometrical characteristics of catalytic bed.

Pellet shape	**Parameter** d_P[mm]	l_P[mm]	D_R [cm]	L_R [cm]
Spheres	1.52	d_P	1.38	1.52
RR	0.83	1.013	1.6	1.27
4HC	0.81	1.013	1.56	1.26

Regarding the RR and $4HC$ were built, imposing that the catalytic bed had the same porosity as in the case of spheres. Also, the catalytic bed constituted by RR and 4HC particles, the pellets distribution, bed porosity and N number is the same as the spheres catalytic bed. The reason to establish the same porosity of the beds constituted by pellets of different geometries, responds to the desire to investigate textural effects due to the different geometries of the catalyst over predictions of pressure drops and further in the comparison of the catalyst activity, neglecting the effects of bed porosity. It is important to mention that based on the concept of symmetry, only half of the domain was considered during calculations.

In this work, the Eulerian two-fluid approach was implemented, where the fluid phases are treated as interpenetrating and the volume averaged governing equations of conservation of mass and momentum are satisfied by each phase (Anderson and Jackson 1967; Ishii 1975). The phase volume fractions (ε_i) concept is used to represent the space occupied by each i-phase and volume fractions are constrained to satisfy $\sum_i \varepsilon_i = 1$. It is important to note that the solid phase is explicitly considered by the geometry of the fixed bed, and its interaction with the fluid phases is considered by adequate boundary condition and the closure for the interchange of momentum between the three phases.

2.2 The continuity and momentum average equation

The continuity equations for the incompressible liquid phase (γ) and compressible gas phase (β) are given by eqs (1) and (2), respectively.

$$\varepsilon_\gamma \rho_\gamma \nabla \cdot \mathbf{v}_\gamma = 0 \qquad \left(\rho_\gamma = cte\right) \tag{1}$$

$$\varepsilon_\beta \nabla \cdot \left(\rho_\beta \mathbf{v}_\beta\right) = 0 \tag{2}$$

Here ρ_i is the scalar density of $i-$ phase and $\mathbf{v}_i$ is the local interstitial velocity vector for the i-phase.

The most appropriate momentum equations for the liquid and gas phases in a TBR that have been previously and successfully used by other researchers (Drew 1983; Froment, F, and Bischoff 1979; Auset and Keller 2004) are,

$$\varepsilon_\gamma \rho_\gamma \left(\mathbf{v}_\gamma \cdot \nabla\right) \mathbf{v}_\gamma = \varepsilon_\gamma \nabla \cdot \left[-P\,\mathbf{I} + \mu_\gamma \left(\nabla \mathbf{v}_\gamma + \left(\nabla \mathbf{v}_\gamma\right)^T\right)\right] + \mathbf{F}_\gamma/\varepsilon_\gamma + \rho_\gamma \mathbf{g} \tag{3}$$

$$\varepsilon_\beta \rho_\beta \left(\mathbf{v}_\beta \cdot \nabla\right) \mathbf{v}_\beta = \varepsilon_\beta \nabla \cdot \left[-P\,\mathbf{I} + \mu_\beta \left(\nabla \mathbf{v}_\beta + \left(\nabla \mathbf{v}_\beta\right)^T\right) - \frac{2}{3}\mu_\beta \left(\nabla \cdot \mathbf{v}_\beta\right)\mathbf{I}\right] + \mathbf{F}_\beta/\varepsilon_\beta + \rho_\beta \mathbf{g} \tag{4}$$

Here, I is the identity matrix, P is the pressure of gas and liquid phases and F_i is the volumetric force term that takes into account the force/momentum exchange between the three phases given by,

$$\mathbf{F}_i = \sum_{j=1}^{n} K_{ji} \left(\mathbf{v}_j - \mathbf{v}_i\right) \tag{5}$$

In eq. (5) the term $\left(\mathbf{v}_j - \mathbf{v}_i\right)$ is the slip velocity between j and i phases and K_{ji} is the momentum exchange coefficient.

To represent liquid-gas, liquid-solid and gas-solid phase interaction, the a) Attou momentum exchange closure (Attou, Boyer, and Ferschneider 1999), on which there is a general consensus that it is adequate to describe the interactions between the phases in TBR's, was used. Although this model has phenomenological bases involving theoretical considerations to evaluate the interaction between the phases in TBR's, actually, the model contains parameters that come from experimental data correlations; in fact, values recommended by Mc Donald et al. for Ergun constants are 180 and 1.8, which are related to bed, and pellet geometry characteristics are used. Consequently, the Attou model is actually a semi-empirical closure expression, implicating that some information and phenomena that take place are unknown. Moreover, in building the model important geometric simplifications and assumptions, like the gas phase do not interact with the solid, are considered. These simplifications have important consequences in the prediction of hydrodynamic parameters like pressure drops, obtaining relative errors estimations of over 27 %. The authors themselves recognize that model underestimates the drop pressure when the columns operates at high pressures and high superficial gas velocities.

Considering that gas-solid interactions could be underestimated in the Attoud model, the b) Gidaspow (Gidaspow 1994), (c) Wen Yu and (Wen and Yu 1966) models, which are not commonly used for this kind of systems, but exhibit a stronger interaction between these phases, were tested to investigate in this regard. The eqs (6)–(8) shows the IMEMs model tested here,

$$
\begin{aligned}
K_{\beta\gamma} &= \varepsilon_\beta \left[\frac{E_1 \mu_\beta \left(1-\varepsilon_\beta\right)^2}{\varepsilon_\beta^2 d_p^2} \left(\frac{\varepsilon_\omega}{1-\varepsilon_\beta} \right)^{0.667} + \frac{E_2 \rho_\beta \left(\mathbf{v}_\beta - \mathbf{v}_\gamma\right)\left(1-\varepsilon_\beta\right)}{\varepsilon_\beta d_p} \left(\frac{\varepsilon_\omega}{1-\varepsilon_\beta} \right)^{0.333} \right] \\
K_{\beta\omega} &= \varepsilon_\beta \left[\frac{E_1 \mu_\beta \left(1-\varepsilon_\beta\right)^2}{\alpha_\beta^2 d_p^2} \left(\frac{\varepsilon_\omega}{1-\varepsilon_\beta} \right)^{0.667} + \frac{E_2 \rho_\beta \mathbf{v}_\beta \left(1-\varepsilon_\beta\right)}{\varepsilon_\beta d_p} \left(\frac{\varepsilon_\omega}{1-\varepsilon_\beta} \right)^{0.333} \right] \\
K_{\gamma\omega} &= \varepsilon_\gamma \left[\frac{E_1 \mu_\gamma \varepsilon_\omega^2}{\varepsilon_\gamma^2 d_p^2} + \frac{E_2 \rho_\gamma \mathbf{v}_\gamma \varepsilon_\omega}{\varepsilon_\gamma d_p} \right]
\end{aligned}
\tag{6}
$$

$$
K_{\beta\omega} = E_1 \frac{\varepsilon_\omega^2 \mu_\beta}{\varepsilon_\beta d_p^2} + E_2 \frac{\rho_\beta \varepsilon_\omega \left|\mathbf{v}_\beta - \mathbf{v}_\omega\right|}{d_p} \qquad \varepsilon_\gamma < 0.8 \tag{7}
$$

$$
\begin{aligned}
K_{\beta\omega} &= \frac{3\rho_\gamma \varepsilon_\omega \left(1-\varepsilon_\beta\right)}{4 d_P} C_D \left|\mathbf{v}_\omega - \mathbf{v}_\gamma\right| \varepsilon_\gamma^{-2.65} \\
C_D &= \frac{24}{\varepsilon_\gamma \mathrm{Re}_\omega} \left[1 + 0.15 \left(\varepsilon_\gamma \mathrm{Re}_\omega \right)^{0.687} \right]; \; \mathrm{Re}_\omega = \frac{\rho_\gamma d_p \left|\mathbf{v}_\omega - \mathbf{v}_\gamma\right|}{\mu_\gamma}
\end{aligned}
\tag{8}
$$

where μ_i is the i-phase viscosity, C_D is the drag coefficient, $E_1 = 260$ and $E_2 = 2.48$ are the Ergun constants used by Al-Dahhan et al. (Al-Dahhan and Dudukovic 1994).

To evaluate the effect of interaction force term between two fluid phases and a solid one, various study cases were established. Table 2 summarizes the characteristic of each implemented study case.

Table 2: Study cases to determine the effect interphase momentum exchange model (IMEM) for force between phases.

Code used	$K_{\beta\gamma}$	$K_{\beta\omega}$	$K_{\gamma\omega}$
1	A	A	A
2	A	G	A
3	A	W	A

A: Attou/G: Gidaspow/W: We-Yu.
S1 means model with spheres (S) and exchange model currently Attou Attou/Attou (1) for $K_{\beta\gamma}/K_{\beta\omega}/K_{\gamma\omega}$ respectively.

2.3 Mass and energy conservation average equation at the interstitial fluid domain

For a better description of the behavior of a TBR, the simulation of the hydrodynamics of two fluid phases in the catalytic bed was coupled with the mass conservation equations for gas, liquid and solid phases. For the interstitial space of the catalytic bed, the model includes the diffusive and convective mass transport eqs (9) and (10),

$$
\nabla \cdot \left(-\mathrm{D}_i^\beta \nabla \langle C_i^\beta \rangle \right) + \mathbf{v}_\beta \cdot \nabla \langle C_i^\beta \rangle = N_i^{\beta\gamma} / \varepsilon_\beta \qquad (i = H_2,\ H_2S, NH_3) \tag{9}
$$

$$
\nabla \cdot \left(-\mathrm{D}_i^\gamma \nabla \langle C_i^\gamma \rangle \right) + \mathbf{v}_\gamma \cdot \nabla \langle C_i^\gamma \rangle = N_i^{\gamma\beta} / \varepsilon_\gamma \qquad (i = H_2,\ H_2S,\ NH_3,\ R-S,\ R-N) \tag{10}
$$

In the case of volumetric mass exchange of *i-specie* between gas and liquid phases, $\left(N_i^{\beta\gamma}\right)$ is given as $N_i^{\beta\gamma} = K_{g,i}^{\beta\gamma} \left(\langle C_i^\beta \rangle R_g T / H_i - \langle C_i^\gamma \rangle \right)$ and it was satisfied that $N_i^{\beta\gamma} = -N_i^{\gamma\beta}$.

Table 3 shows the operation conditions and physical properties used in the CFD model.

Table 3: Physical properties and operating conditions used in the CFD model.

Bed and catalyst properties

ε_B	$0.41 - 0.49$	N	$D_R/d_P \simeq 9.1,\ 18.4$
ε_γ	$0.1 - 0.18$	d_P	1.52, 0.31 mm
ε_σ	0.4535	a_v	1110.1 m^{-1}
Physical properties at 0.31 MPa and 598 K			
ρ_{Hexane}	586.5 kg/m^3	ρ_{N_2}	3.5 kg/m^3
μ_{Hexane}	2.95×10^{-4} Pa · s	μ_{N_2}	1.77×10^{-5} Pa · s
Physical properties at 3.55 MPa and 598 K			
ρ_{Hexane}	591.1 kg/m^3	ρ_{N_2}	39.7 kg/m^3
μ_{Hexane}	3.039×10^{-4} Pa · s	μ_{N_2}	1.813×10^{-5} Pa · s
Physical properties at 10 MPa and 623.15 K			
ρ_{Gasoil}	705.9 kg/m^3	ρ_{H_2}	3.79 kg/m^3
μ_{Gasoil}	2.969×10^{-4} Pa · s	μ_{H_2}	1.47×10^{-5} Pa · s
C_A^0	54.8 mol/m^3	$K_{H_2S}^{\beta\gamma}$	$6.29 \times 10^{-2}\ 1/s$
D_{R-S}^{γ}	$3.25 \times 10^{-9}\ m^2/s$	$K_{H_2}^{\beta\gamma}$	$5.72 \times 10^{-2}\ 1/s$
$D_{H_2S}^{\gamma}$	$1.10 \times 10^{-8}\ m^2/s$	$K_{NH_3}^{\beta\gamma}$	$0.208\ 1/s$
$D_{H_2}^{\gamma}$	$1.33 \times 10^{-8}\ m^2/s$	$K_{H_2S}^{\gamma\omega}$	8.464×10^{-6} m/s
$D_{NH_3}^{\gamma}$	$1.003 \times 10^{-9}\ m^2/s$	$K_{NH_3}^{\gamma\omega}$	1.204×10^{-6} m/s
$D_{H_2S}^{\beta}$	$2.37 \times 10^{-6}\ m^2/s$	H_{H_2}	17, 676 Pa m^3/mol
$D_{H_2}^{\beta}$	$1.79 \times 10^{-8}\ m^2/s$	H_{H_2S}	214, 673 Pa m^3/mol
$D_{NH_3}^{\beta}$	$2.3 \times 10^{-6}\ m^2/s$	H_{NH_3}	44, 450.2 Pa m^3/mol
$-\Delta H_{HDS}$	251 kJ/mol	MW_{gasoil}	319.98 g mol^{-1}
d_b (Mitra 2011)	5 mm		

For the evaluation of some properties of Light Gasoil (LGO), and H_2 and H_2S, some correlations found in the literature (Chacón et al. 2012; Katz et al. 1959; Mederos and Ancheyta 2007; Ahmed 1989) were used and these are shown in Table 4. Larachi's pressure drop correlation was used to evaluate the liquid holdup as initial input to the CFD model and to evaluate the velocities when liquid holdup equalized with our CFD simulations.

Table 4: Correlations to estimate properties of gasoil and gases used in the CFD model.

Parameter	Correlation
Gasoil density (Mederos and Ancheyta 2007)	$\rho_{gasoil}\left[kg/m^3\right] = \rho_0 + 16.0185\left(\Delta\rho_P - \Delta\rho_T\right)$ $\Delta\rho_P = \left[0.167 + 16.181\times10^{-0.965913\rho_0}\right]\left[\frac{P}{6893984}\right] - 0.01\left[0.299 + 263\times10^{-0.00376441\rho_0}\right]\left[\frac{P}{6893984}\right]^2$ $\Delta\rho_T = \left[0.0133 + 154.4\left(\frac{\rho_0}{16.0185} + \Delta\rho_P\right)^{-2.45}\right]fT_\gamma - \left[8.1\times10^{-6} - 0.0622\times10^{-0.764(0.062428\rho_0+\Delta\rho_P)}\right]\left(fT_\gamma\right)^2$ $fT_\gamma = 1.8T_\gamma - 520$
Henry coefficient (Mederos and Ancheyta 2007)	$H_i\left[\frac{m^3Pa}{mol}\right] = \frac{V_N}{\lambda_i\,\rho_{gasoil}}$
Solubility of H_2 (Mederos and Ancheyta 2007)	$\lambda_{H_2}\left[\frac{lt}{Pa\cdot kg}\right] =$ $\left[-0.5597 - 0.4295\times10^{-3}T_\gamma + 3.0754\times10^{-2}\frac{T_\gamma}{\rho_{20}} + 1.9459\times10^{-6}T_\gamma^2 + \frac{8.3578\times10^{-8}}{\rho_{20}^2}\right]\times 10^{-6}$
Solubility of H_2S (Mederos and Ancheyta 2007)	$\lambda_{H_2S}\left[\frac{lt}{Pa\cdot kg}\right] = \exp\left(3.367 - 0.00847T_\gamma\right)\times10^{-6}$
Dynamic liquid viscosity (Ahmed 1989)	$\mu_\gamma = 3.141\times10^{10}\left(T_\gamma - 460\right)^{-3.444}\left[\log_{10}\left(API\right)\right]^a,\ a =$ $10.313\left[\log_{10}\left(T_\gamma - 460\right)\right] - 36.447$
Diffusivity (Mederos and Ancheyta 2007)	$D_i^\gamma\left[\frac{m^2}{s}\right] = 9.01263\times10^{-16}\left(\frac{V_\gamma^{0.267}}{V_i^{0.433}}\right)\left(\frac{T_\gamma}{\mu_\gamma}\right),\ V_\gamma = \frac{MW}{1000\rho_0}$
Molar Volume (Mederos and Ancheyta 2007)	$V_i\left[\frac{m^3}{mol}\right] = 1.4684\times10^{-13}V_c^{1.048}$
Liquid holdup (Al-Dahhan and Dudukovic 1994)	$\varepsilon_\gamma = \varepsilon_B\left(\frac{E_1Re_\gamma^{**} + E_2Re_\gamma^{**2}}{Ga_\gamma\left(1+\frac{\Delta P^*}{\rho_\gamma g}\right)}\right)^{1/3},\ Re_\gamma^{**} = \frac{Re_\gamma^*}{(1-\varepsilon_B)},\ Ga_\gamma =$ $\frac{g\,{D_p}^3{\varepsilon_B}^3{\rho_\gamma}^2}{{\mu_\gamma}^2(1-\varepsilon_B)^3}$
ΔP* Larachi correlation (Larachi et al. 1991)	$\Delta P^* = \frac{2G^2}{dh\,\rho_\beta}\left[\frac{1}{\kappa^{1.5}}\left(31.3 + \frac{17.3}{\kappa^{0.5}}\right)\right],\ \kappa = X_\beta\left(Re_\gamma^*\,We_\gamma\right)^{0.25},\ Re_\gamma^* = \frac{\rho_\gamma V_\gamma D_p}{\mu_\gamma}$ $X_\beta = \frac{G}{L}\left(\frac{\rho_\gamma}{\rho_\beta}\right)^{0.5},\ We_\gamma = \frac{L^2D_p}{\rho_\gamma\sigma_\gamma},\ dh = \left(\frac{16{\varepsilon_B}^3}{9\pi(1-\varepsilon_B)^2}\right)^{1/3}D_p$
Molar Volume (Mederos and Ancheyta 2007)	$V_i\left[\frac{m^3}{mol}\right] = 1.4684\times10^{-13}V_c^{1.048}$
Liquid-solid mass transfer coefficients (Goto and Smith 1975)	$\frac{K_i^{\omega\gamma}}{a_S}\left[cm/s\right] = 0.0018\left(\frac{G}{\mu_\gamma a_S}\right)^{1/2}\left(\frac{\mu_\gamma}{\rho_\gamma D_i^\gamma}\right)^{1/3}$
Gas-liquid mass transfer coefficients (Specia, Baldi, and Gianetto 1978)	$\frac{K_i^{\beta\gamma}a_L}{D_i^\gamma}\left[\frac{1}{s}\right] = 1.1094\times10^{-3}\left(\frac{G}{\mu_\gamma}\right)^{0.4}\left(\frac{\mu_\gamma}{\rho_\gamma D_i^\gamma}\right)^{0.5}$

2.4 Bed domain mass conservation average equation

In the case of solid domain, the mass conservation equations consider diffusive transport and generation due to reaction. Then to model the mass transport in the catalyst that constitute the packed bed, the diffusion-reaction averaged equation, (11), are required to be satisfied in the solid domain (Lopes and Quinta-Ferreira 2010a; 2010b) which is actually a pseudo-phase (ω-*pseudophase*) consisting of the catalytic solid matrix (σ-*phase*) and because of capillary forces (Chacón et al. 2012) we assume that the liquid phase(λ-*phase*) fills the interstices left by the solid matrix of the catalytic pellets. The latter implies that the interstices are assumed to be completely wet.

$$\nabla \cdot \left(-\varepsilon_\lambda \mathbf{D}^{\omega}_{eff,i} \nabla \langle C^{\omega}_i \rangle^{\omega} \right) = \nu_i \langle r^{\omega}_j \rangle^{\omega} \quad (i = H_2,\ H_2S,\ R-S, R-N, NH_3) \tag{11}$$

The details on the evaluation of effective transport coefficients have been reported in a previous work (Cordero et al. 2014; Whitaker 1999) and the reactions rate for HDS and HDN and are given by eqs 14 and 15, and. The brackets imply that the pellets are considered as pseudo-homogeneous domain and the property inside is an average quantity valid in all catalytic domains. Also, the superscript ω implies that the considered average is the superficial average (Whitaker 1999).

2.5 Kinetic model

The HDS and HDN reactions of light Gasoil that takes place in the reactor above described, satisfy the following stoichiometric relationship,

$$\nu_{R-S} R-S_{(liq)} + \nu_{H_{2,\,1}} H_{2(g)} \rightarrow \nu_{R-H_2} R-H_{2(liq)} + \nu_{H_2S} H_2S_{(g)} \tag{12}$$

$$\nu_{R-N} R-N_{(liq)} + \nu_{H_{2,\,2}} H_{2(g)} \rightarrow \nu_{R-H_3} R-H_{3(liq)} + \nu_{NH_3} NH_{3(g)} \tag{13}$$

where $\nu_{R-S} = -1$, $\nu_{H_{2\,,1}} = -2$, $\nu_{R-H_2} = 1$, $\nu_{H_2S} = 1$, $\nu_{R-N} = 1$, $\nu_{H_{2\,,2}} = 3$, $\nu_{R-H_3} = -1$, $\nu_{NH_3} = -1$ and $\nu_{NH_3} = -1$

In this work, the kinetics for HDS and HDN process for LGO follow LHHW type expressions where the sulfurized, nitrated species and the hydrogen are assumed to chemisorb on the active sites (Chacón et al. 2012).

$$-r_{HDS} = \frac{k_{HDS} \langle C^{\omega}_{RS} \rangle^{\omega} \left(\langle C^{\omega}_{H_2} \rangle^{\omega} \right)^{0.5}}{\left(1 + K_{H_2S} \langle C^{\omega}_{H_2S} \rangle^{\omega} \right)^2} \tag{14}$$

$$-r_{HDN} = \frac{k_{HDN} \langle C^{\omega}_{RN} \rangle^{\omega} \langle C^{\omega}_{H_2} \rangle^{\omega}}{\left(1 + K_{NH_3} \langle C^{\omega}_{NH_3} \rangle^{\omega} \right)^2} \tag{15}$$

Table 5 shows the used kinetic parameters (Chacón et al. 2012).

Table 5: Kinetic parameters for HDS and HDN reactions.

$k_{HDS}\left[\left(\frac{\mathrm{m}^3}{\mathrm{mol}}\right)^{0.5}/s\right] = k^0_{HDS} e^{(-E_{HDS}/R_g T)}$	$k_{HDN}\left[\mathrm{m}^3/\mathrm{mol}\cdot\mathrm{s}\right] = k^0_{HDN} e^{(-E_{HDN}/R_g T)}$
$k^0_{HDS}\left[\left(\frac{\mathrm{m}^3}{\mathrm{mol}}\right)^{0.5}/s\right] = 6.46125 \times 10^{-5}$	$k^0_{HDN}\left[\mathrm{m}^3/\mathrm{mol}\cdot\mathrm{s}\right] = 3.26268$
$E_{a,HDS}\,[\mathrm{J/mol}] = 90,180$	$E_{a,HDN}\,[\mathrm{J/mol}] = 80,680$
$K_{H_2S}\left[\mathrm{m}^3/\mathrm{mol}\right] = k^0_{H_2S} e^{(Q_{H_2S}/R_g T)}$	$K_{NH_3}\left[\mathrm{m}^3/\mathrm{mol}\right] = k^0_{NH_3} e^{(Q_{NH_3}/R_g T)}$
$k^0_{H_2S}\left[\mathrm{m}^3/\mathrm{mol}\right] = 0.038$	$k^0_{NH_3}\left[\mathrm{m}^3/\mathrm{mol}\right] = 2.55 \times 10^{-11}$
$Q_{H_2S}\,[\mathrm{J/mol}] = 2,530$	$Q_{NH_3}\,[\mathrm{J/mol}] = 111,000$

2.6 Boundary conditions

The CFD model coupling three phase mass and two-phase momentum averaged transport equations satisfies the set of boundary conditions shown in Table 6.

Table 6: Boundary conditions used in the CFD model.

Hydrodynamics ($f = \gamma, \beta$ *phases*)		
$\mathbf{v}_f = -\mathbf{n}\, v_f^0$ (inlet velocity)	at reactor inlet $z = L_R$	(16)
$P = -P^{op}$, $\mathbf{n}\left[\mu_f\left(\nabla\mathbf{v}_f + \left(\nabla\mathbf{v}_f\right)^T\right)\right] = 0$ (outlet pressure, non-viscous stress)	at reactor outlet $z = 0$	(17)
$\mathbf{v}_f = 0$ (no slip)	at solid-fluid interphase $A_{j\omega}$	(18)
$\mathbf{v}_f = 0$ (no slip)	at reactor walls $r = r_R$	(19)
$\mathbf{n}\cdot\mathbf{v} = 0$, $\mathrm{K} - (\mathrm{K}\cdot\mathbf{n})\,\mathbf{n} = 0$ (symmetry)	at central plane in the axial direction ($z = 0$)	(20)
Mass transport at gas domain($i = H_2,\ H_2S, NH_3$)		
$\langle C_{H_2}^{\beta}\rangle = C_{H_2}^0$, $\langle C_{H_2S}^{\beta}\rangle = \langle C_{NH_3}^{\beta}\rangle = 0$	at reactor inlet $z = L_R$	(21)
$-\mathbf{n}\cdot \mathrm{D}_i^{\beta}\nabla\langle C_i^{\beta}\rangle = 0$ (only covective flux)	at reactor outlet $z = 0$	(22)
$-\mathbf{n}\cdot\mathbf{N}_i^{\beta} = 0$ (impermeability)	at reactor walls $r = r_R$	(23)
$-\mathbf{n}\cdot\mathbf{N}_i^{\beta} = 0$ (symmetry)	at central plane in the axial direction	(24)
Mass transport at liquid domain($i = H_2,\ H_2S,\ NH_3, R-S, R-N$)		
$\langle C_{R-S}^{\gamma}\rangle = C_{R-S}^0$, $\langle C_{R-N}^{\gamma}\rangle = C_{R-N}^0$, $\langle C_{H_2}^{\gamma}\rangle = \langle C_{H_2S}^{\gamma}\rangle = \langle C_{NH_3}^{\gamma}\rangle = 0$	at reactor inlet $z = L_R$	(25)
$-\mathbf{n}\cdot \mathrm{D}_i^{\gamma}\nabla\langle C_i^{\gamma}\rangle = 0$ (only covective flux)	at reactor outlet $z = 0$	(26)
$-\mathbf{n}\cdot\mathbf{N}_i^{\gamma} = 0$ (impermeability)	at reactor walls $r = r_R$	(27)
$-\mathbf{n}\cdot\mathbf{N}_i^{\gamma} = -\mathrm{D}_{eff,\,\mathrm{i}}\nabla\langle C_i^{\omega}\rangle^{\omega}$ (flux continuity)	at solid-fluid interphase $A_{\gamma\omega}$	(28)
$-\mathbf{n}_i\cdot\mathbf{N}_i^{\beta} = 0$ (symmetry)	at central plane in the axial direction	(29)
Mass transport at solid domain($i = H_2,\ H_2S, NH_3, R-S, R-N$)		
$\langle C_i^{\omega}\rangle^{\omega} = \langle C_i^{\gamma}\rangle$ (concentration continuity)	at solid-fluid interphase $A_{\gamma\omega}$	(30)
$-\mathbf{n}\cdot\mathbf{N}_i^{\omega} = 0$ (flux continuity)	at catalyst centers	(31)

Here the total mass flux is given by: $\mathbf{N}_i^j = -\mathrm{D}_i^f\nabla\langle C_i^f\rangle + \mathbf{v}_i\langle C_i^f\rangle$

Here the subscript f represents both gas and liquid phases flowing inside the TBR.

2.7 Model assumptions

This model considers that the reactor operates in a Trickle regime where the gas and liquid co-currently flow and for HDS analysis, due to the reactor small dimensions($L_R \approx 0.7$cm, $D_R \approx 0.64$ cm) the temperature gradients are expected to be very small and it can be assumed that the reactor operates isothermally (Chacón et al. 2012). Due that the pressure gradient ($\Delta P \approx 16$ Pa) for the model that couple hydrodynamics with mass transport is very small, the density and viscosity of gas and liquid phases are considered constant.

Also, it was assumed that the catalyst activity does not change with time and vaporization and condensation of gasoil do not take place. Chemical reactions take place only at the solid catalyst which is considered to be completely wet, for purposes of mass transport model. As for the selection of the value of $N = D_R/d_P$, this was done based on a literature review, regarding critical values used in CFD models (Beni and Khosravi-Nikou 2016; Lopes and Quinta-Ferreira 2010b; Dorai et al. 2015; García-Martínez et al. 2015). On the other hand, according to Beni et al. (Beni and Khosravi-Nikou 2016), the importance of wall effects due to bypass flows of reactants are present in a region of a typical width of 2–3 pellet diameters. They also affirm that it has been observed that at very low particle diameter ratio (between 7–10), dispersion is smaller than for larger ratios. This phenomenon is known as the Knox Parcher effect and they suggest that a minimum bed height of about 15 particle diameters is required for dispersive plug-in model to be valid. Then, a value of $N \approx 10$ is considered sufficient for an accurate prediction of both, pressure drop and holdup. A brief discussion about the results in this regard that supports the N selection is presented within the results section.

Regarding the reactor length of our model, in literature there are several criteria regarding the L_R/d_p ratio to ensure that there is no axial dispersion. It can be mentioned that according to Mears there are no simple rules and criteria suitable for all cases (García-Martínez et al. 2015). In spite of this, for example Gianetto and Specchia

propose $L_R/d_p > 15 - 20$ (Gianetto and Specchia 1992). On the other hand, implementing a CFD reactor model of industrial or pilot reactors scales would be a complicated task due to the great computational resources that would be needed. Therefore, due to computational limitations, the length $\left(L_R/d_p \simeq 20\right)$ considered in the reactor model constructed here is considered as representative.

It is considered that the ordered catalyst bed representation built for the model contains enough characteristics of a real catalytic bed. It is important to highlight that in the pseudo-homogeneous models commonly found in literature, the only considered information of the bed is its porosity. Regarding to this point, tens of scientific works where simplified geometries of porous media give acceptable results to capture the essence of these systems, in several kinds of phenomena and applications (Dorai et al. 2015; Cordero et al. 2014; Whitaker 1999; Lugo-Méndez et al. 2015; Gujal, Ranade, and Chaudhari 2005) can be found in literature. Even more, an important aspect in approaches like volume averaging method, which allows to deal with complexities found in multi-scale phenomena and porous media, is precisely the validity of the unit cells geometrical representations of porous media, that however lead to result with acceptable accuracy. The construction of a more realistic and random geometry implies a greater complexity and it is left for a later study.

Since in the geometrical model for the bed built here, the variation in porosity is explicitly considered, no expression of porosity variation across the column radius is necessary to take account their effect over TBR behavior. In addition, the effect of porosity variations on the hydrodynamic and kinetic behavior of TBR is part of the aspects studied, discussed and analyzed with great detail in this work.

Regarding the validity of symmetry assumption, works that deal with this and suggest critical values where the symmetry plane is loosed can be found in the literature. However, the systems studied are very simple, considering the flow through a unique submerged particle with values of $210 < \mathrm{R}e_C < 270$ (Mital 1998) and $\mathrm{R}e_C > 275$ (Chrust, Goujon-Durand, and Wesfried 2013). TBR systems are more complex than those aforementioned, involve two fluid phases considered as interpenetrating and interacting with one third solid phase constituted by a multitude of solid bodies submerged, and in literature no analysis of the validity of symmetry can be found for such complex systems, thus its considered that the symmetry assumption is valid, and the accuracy of the results support this assumption and all others referring to the geometric simplifications of the catalytic bed.

3 Results and discussion

The model was implemented in the commercial CFD software COMSOL Multiphysics 5.2, running in a Microsoft operating system MS Windows 10, in a workstation equipped with two Intel® Xeon® E5-2603 v3 processor with four cores each, at 1.6 GHz and 160 GB of RAM memory. Further tests concerning results independence with the mesh size were made, in order to achieve fields with reasonable convergence, about $\sim 6 \times 10^6$ mesh elements were required. Some details regarding the computational resources and times required in the simulations are presented in Table 7.

Table 7: Details of the computing resources required in each CFD model.

Model	Number of tested cases	Mesh $\left[\begin{smallmatrix}Triangular\\elements\end{smallmatrix}\right]$	Maximum in RAM memory [GB]	Maximum in Virtual memory [GB]	Computing time* [hr]
Hydrodynamics	216[a]	3.23×10^6	~ 14	~ 25	1.74–19
Hydrodynamics coupled with mass transfer	56[b]	6×10^6	~ 80	~ 110	504–168

*Depending on the particular simulation/case tested.
[a]Considering all geometries, IMEMs, pressures, and comparison cases and data points tested.
[b]Considering all effective diffusivities, variations in operation conditions and in inflows tested, only for the spheres cases.

For hydrodynamics simulations, features of the TBR geometric model, were selected in concordance with experimental data from Al-Dahhan et al. (Al-Dahhan and Dudukovic 1994), that is, bed porosity of $\varepsilon_B = 0.41$, particle diameter of $d_P = 1.52\,\mathrm{mm}$ gas velocity of $v_\beta^0 = 8.5\ \mathrm{cm/s}$, and liquid mass velocity range of $L = 0.81 - 1.95\ \left[\mathrm{kg/m^2 s}\right]$, and the fluids considered were hexane and nitrogen, therefore the physical properties were the same (see Table 3).

To validate the results, the two fluid phase hydrodynamics simulations were compared with experimental and theoretical pressure drop and liquid holdup data of high and low-pressure operation (Al-Dahhan and Dudukovic 1994; Attou, Boyer, and Ferschneider 1999). It is worth noticing, however, that this CFD model is far from the Al-Dahhan's experimental system in the ratio diameter to length of packed bed and pellet to column diameters; while the Al-Dahhan's experimental column has a catalyst to reactor diameter ratio of N = 14.6; ours was selected to be N = 9.1. Since the column with which it is compared has different diameter and length, it is not possible to establish simultaneously the same phase interstitial velocities or mass velocities and the same residence times (LHSV/GHSV). Then for comparison purpose, four study cases were established, and both columns were compared equaling i) hourly spatial velocities (LHSV/GHSV), ii) gas and liquid mass flow velocities (L-G), iii) liquid and gas phase Reynold numbers (Re_γ-Re_β), and iv) liquid holdup (ε_γ).

Figure 2 shows the predicted values of dimensionless pressure drop (ψ) compared against experimental literature data, for both high and low-pressure operation and for the four cases used to compare the reactor model with Al-Dahhan's column. Liquid mass flow rates values (L) according experimental setup developed in literature are shown (Al-Dahhan and Dudukovic 1994), and finally the liquid Reynold numbers (Re_γ), liquid hourly space velocity ($LHSV$) and liquid holdup (ε_γ), corresponding to this L values for both high and low-pressure operation are presented. These data are the values used to compare the literature column with the reactor model, which as previously mentioned have different lengths and diameters. To exemplify how we proceeded, considering the series called LHSV-GHSV implies that in the CFD simulations was fed with the same values of those parameters than the ones calculated from the values of L and v_β^0 specified in the experimental setup of Al-Dahhan. That is, both Al-Dahhan model and ours have the same values of LHSV and GHSV, but do not share the same values of the other parameters of that table *(L–G, Re_γ– Re_β, and ε_γ–ε_β)*. In the same way, Re_γ– Re_β series implies that our model takes the same values of these parameters than those of the Al-Dahhan's model, which were estimated from their respective L and $\mathbf{v}_\beta$ values, and again, the two columns cannot satisfy at the same time the equality in the other parameters *(L–G, LHSV-GHSV, and ε_γ–ε_β)*.

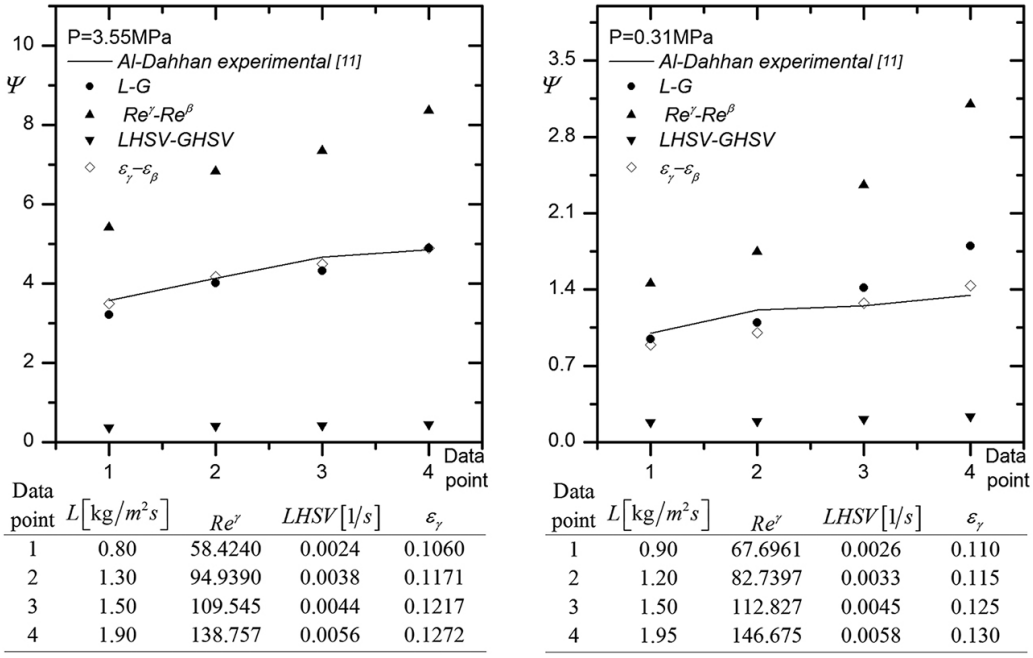

Data point	$L\left[\mathrm{kg}/m^2s\right]$	Re^γ	$LHSV\left[1/s\right]$	ε_γ
1	0.80	58.4240	0.0024	0.1060
2	1.30	94.9390	0.0038	0.1171
3	1.50	109.545	0.0044	0.1217
4	1.90	138.757	0.0056	0.1272

Data point	$L\left[\mathrm{kg}/m^2s\right]$	Re^γ	$LHSV\left[1/s\right]$	ε_γ
1	0.90	67.6961	0.0026	0.110
2	1.20	82.7397	0.0033	0.115
3	1.50	112.827	0.0045	0.125
4	1.95	146.675	0.0058	0.130

Figure 2: Comparison of dimensionless pressure drop$\Psi = (\Delta P/m)/\rho_\gamma g$ predicted values at high(3.55 MPa) and low(0.31 MPa) pressure operation against Al-Dahhan's experimental data (Al-Dahhan and Dudukovic 1994), all data presented have $v_\beta^0 = 8.5$ cm/s.

The results show that the best predictions of dimensionless pressure drop are obtained by equaling the liquid holdup and mass flow rates in both columns, with MAREs of 1.9 and 5.23 per cent respectively for high-pressure operation, and 8.89 and 15.4 per cent for low-pressure operation. Also, it is evident that the worst predictions are obtained by equalizing the hourly spatial velocities whit MAREs of 90.2 and 82.7 per cent for high and low-pressure operation respectively, even though equaling LHSV and GHSV is the most common technique used to scale up and compare the behavior of two reactors with different diameters and lengths (Dorai et al. 2015).

Figure 3 shows parity plots for liquid holdup, used to validate the predicted values against Al-Dahhan's experimental data (Al-Dahhan and Dudukovic 1994). Each series of this figure correspond to the four methods established to compare both columns as it was previously mentioned, and the four points of each series

correspond to the data points shown in Figure 2 and which description was done. In all simulations, the value of v^0_{β}=0.85 cm/s was specified. The IMEM tested and shown in Figure 2 and Figure 3 correspond to S1 case, which description is shown in Table 2.

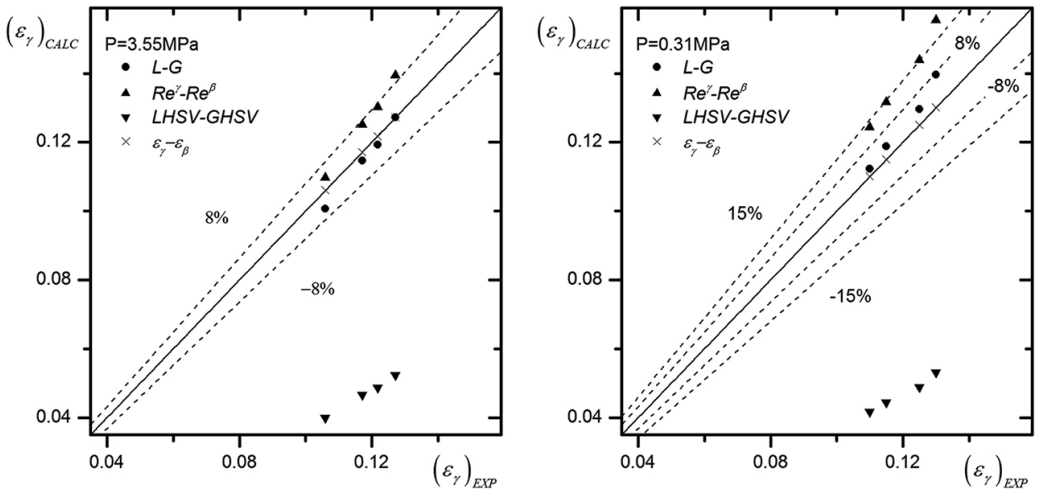

Figure 3: Parity plot of liquid holdup predicted values validation at high(3.55 MPa) and low(0.31 MPa) pressure operation for the four cases of comparison of Al-Dahhan and the column model.

As in the case of pressure drop, equaling the hourly space velocities lead to the worst prediction with MAREs of 152 and 156 % respectively for both low and high-pressure operation; this is particularly noteworthy since the estimation of liquid holdup is traditionally very accurate in the literature (Carbonell 2000). The above suggests that the technique of equaling the LHSV-GHSV for the scaling-up process does not lead to the same values of hydrodynamic key parameters in two reactors with different diameters and lengths as is usually considered. On the other hand, equaling the mass velocity lead to MAREs of 2 and 4 per cent for high and low pressure operation respectively, implying that both columns have a more similar liquid holdup and pressure drop values despite differences in diameter and length; So if a similar holdup and pressure drop values is sought between two columns of different characteristic lengths, equaling the liquid holdup or the mass velocities lead to better results.

It is important to mention that the validation of the model is not trivial because once the hydrodynamic model is validated, it is possible to couple other features like chemical species and energy transport and chemical reaction, and only a model including all these phenomenological characteristics will provide criteria to understand and improve TBR performance (Partopour and Dixon 2016).

In this sense, Figure 4(a) shows the MAREs for the comparison of dimensionless pressure drop and HDS reaction conversion between the reactor model and Al-Dahhan's hydrodynamic experimental data, and Chacon's kinetic theoretical study (Al-Dahhan and Dudukovic 1994; Chacón et al. 2012) for a catalytic bed constituted by spherical pellets of 0.35 mm, and considering a S1 IMEM. It is important to highlight that due to differences of length scales between both compared reactors, the four comparison cases were tested and the results are also shown in Figure 4(a).

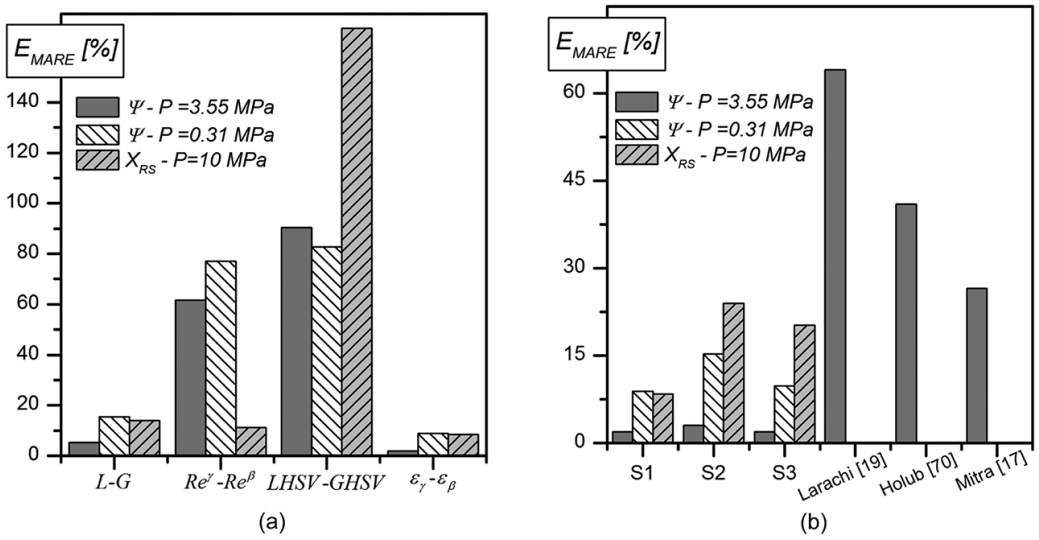

Figure 4: (a) MAREs for dimensionless pressure drop and HDS conversion using the four cases tested to compare the TBR model against literature models (Al-Dahhan and Dudukovic 1994; Chacón et al. 2012). (b) MAREs for dimensionless pressure drop and HDS conversion using different IMEM comparing with literature predicted values (Al-Dahhan and Dudukovic 1994; Chacón et al. 2012).

For HDS and HDN simulations, the geometric model used to simulate the hydrodynamics was adapted leading to the following dimensions$L_R \simeq 0.69$ cm and $D_R \simeq 0.64$ cm, for comparison purposes with the model reported by Chacon et al (Chacón et al. 2012), who conducted an isothermal and stationary reactor simulation of a light gas oil hydrodesulphurization and who compared their results with experimental data from Botchwey (Botchwey, Dalai, and Adjaye 2003).

Chacon's model considers that i) the gas and liquid velocities are constants along the reactor, ii) there is not a concentration profile in the radial direction, iii) the internal mass transfer inside the catalyst particle (internal diffusion) is described through the catalyst effectiveness factor, which varies with the conversion along the reactor, and iv) that the thermodynamic equilibrium is described through Henry's Law.

At this point it is worth noticing that in the proposed model there is no need to assume constant gas and liquid phase velocities, neither restrict the transport of mass in the radial direction or in any other direction of the reactor, and also, the model takes into account the mass resistances inside the catalyst domain, and the model does not assume that the pressure is constant; in fact, this is a variable evaluated in the simulations and it is of paramount importance in the design of a TBR and the conversion predicted by the TBR models.

Again, comparing the Chacón reactor with ours through equalizing the liquid Holdup and the mass velocities, lead to the best predictions, with absolute relative error at reactor outlet of 5.83 and 5.12 percent respectively, implying that the same conversion values are obtained between two reactors of different dimensions by equaling these parameters. While equaling of the hourly space velocities leads to the worst predictions with deviations of 167.5 %, suggesting that using this way of comparing the two reactors, similar conversion values prediction are not obtained between them. For HDN reaction a similar trend is found, equalizing the liquid Holdup conduces to best predictions and equalizing LHSV and GHSV to the worst. The above is very significant since it is precisely by equaling the LHSV and GHSV that scale up process is usually made (Dorai et al. 2015).

Figure 4(b) shows the MAREs of simulations that uses the IMEMs shown in Table 2 against Al-Dahhan's experimental data (Al-Dahhan and Dudukovic 1994); and for comparison proposes, the predicted values of three literature works are shown (Holub, Dudukovic, and Ramachandran 1992; Iliuta and Larachi 1999; Mitra 2011). Models S1, S2 and S3 give excellent predictions for pressure drop, with MARE below 3.1 %; In fact, the conventional model (S1) leads to excellent predictions with a MARE of 1.9 % when the holdups are equalized, and of 1.95 % when mass velocities are equalized. This implies 25 % better accuracy in predicting dimensionless pressure drops in operation at low pressure and an improvement of five times at high pressures operation, in comparison with literature works (Al-Dahhan and Dudukovic 1994; Atta, Shantanu, and Nigam 2009; Holub, Dudukovic, and Ramachandran 1992; Iliuta and Larachi 1999; Mitra 2011; Solomenko et al. 2015). While when the Reynolds number and hourly space velocities are used to compare both reactors with S1 IMEM model, the MARE´s obtained are 62 % and 90.2 % respectively. Figure 4(b) also shows the MARE's obtained for HDS conversion using S1, S2 and S3 IMMEM's models, obtaining the lowest deviation of HDS conversion of 5.12 % in comparison with Chacon work (Chacón et al. 2012) for the IMEM S1, and correspond to the comparison of Chacón column and ours by equaling the liquid and gas mass velocities *(L-G)*.

Is important to note that the excellent accuracy in pressure drop prediction is due the conjunction of three aspects: 1) a suitable IMEM (the Attou model) to describe the interaction between phases in the TBR, incorporating gas-solid interaction 2) the incorporation of more geometrical details of the catalytic bed, and 3) a correct form to compare two TBR's with different length scales (a suitable scaling-up procedure). The excellent results in predictions also, support the validity of assumptions and simplifications made in establishing of the model.

On the other hand, it should be emphasized that the model was validated against two totally different systems: a cold column (hexane-nitrogen) where 8 pressure drop and 8 liquid holdup data were compared for both low and high operating pressures, and a TBR (light gasoil-hydrogen) where 12 conversion data were compared for both HDS and HDN reactions. Thus, it can be concluded that the CFD model is capable of adequately reproducing the hydrodynamic and kinetic behavior of a TBR and that the possibility of a coincidence is very remote.

On another hand, the already validated hydrodynamic model, allows to extrapolate other studies regarding hydrodynamics, like the effects of the catalyst geometry and bed porosity. Figure 5(a) and Figure 5(b) show the values of pressure drop and liquid holdup both at low and high pressure for sphere catalyst and with beds with porosities of 0.41 and 0.48 respectively. In both, the three IMEMs tested were compared with the hydrodynamic parameters determined by Al-Dahhan (Al-Dahhan and Dudukovic 1994) for a porosity of 0.41, which are also presented in Figure 5(a). For the case of spherical particles of porosity of 0.41, the range of values of dimensionless pressure drops in the liquid holdup range of (0.106–0.1272) for operation at high pressures

are (3.421–4.8), (3.499–4.892) and (3.519–4.930) for IMEM's S4, S1 and S7, respectively. While in operation at low pressure in the liquid holdup range of (0.11–0.13) the dimensionless pressure drops are in the range of (0.793–1281), (0.8943–1.4337) and (0.9055–1.481).

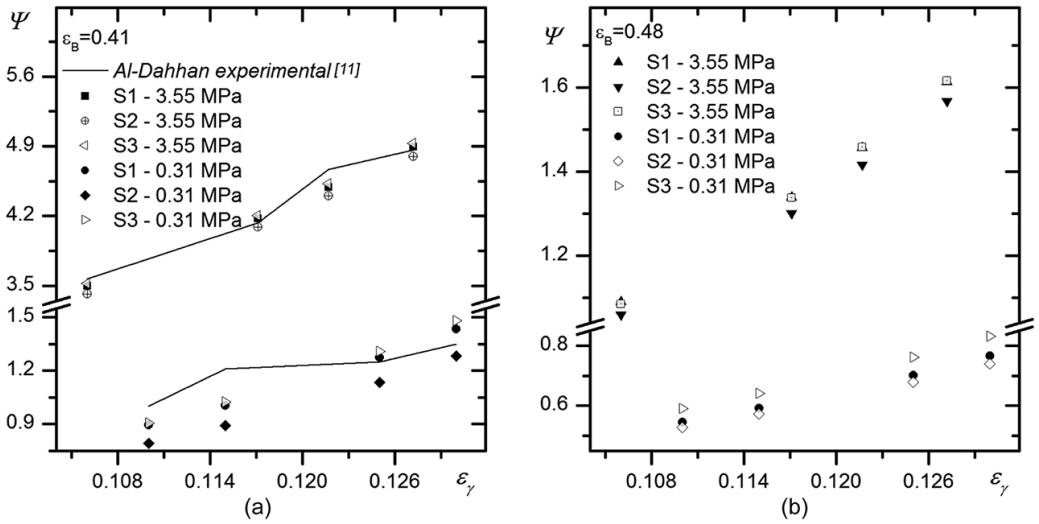

Figure 5: (a) Dimensionless pressure drop in a bed of spherical particles with bed porosity of 0.41, using IMEMs S1, S4 and S7 at different liquid holdups; and comparison against experimental literature data. (b) Dimensionless pressure drop in a bed with spherical particles with bed porosity of 0.48, using IMEMs S1, S4 and S7 at different liquid holdups.

Figure 6(a) and Figure 6(b) show the predicted values of pressure drop both at low and high pressure operation for Raschig rings catalyst (RR) and with beds with porosities of 0.48 and 0.49 respectively at different liquid holdups values and with the different IMEMs tested; while Figure 6(c) and Figure 6(d) show the same details, but with four hole cylindrical pellets (4HC). From Figure 5(b), Figure 6(a) and Figure 6(c), for both high and low operation pressure, the same behavior can be observed, the highest dimensionless pressure drop estimations (high-pressure range – low-pressure range) are obtained for RR particles (1.723–2.466, 0.808–1.241), followed by 4HC (1.355–1.991, 0.729–1.090), and lastly spherical particles (1.089–1.613, 0.545–0.765). Same behavior can be observed in Figure 6(b) and Figure 6(d) for RR and 4HC with a bed porosity of 0.49. The variation due to the geometry in pressure drop in reference to spherical particles bed with porosity of 0.48, are 150.34 % and 66.2 % for RR and 4HC respectively, at high pressure operation, and 75.05 % and 51.92 % at low pressure operation.

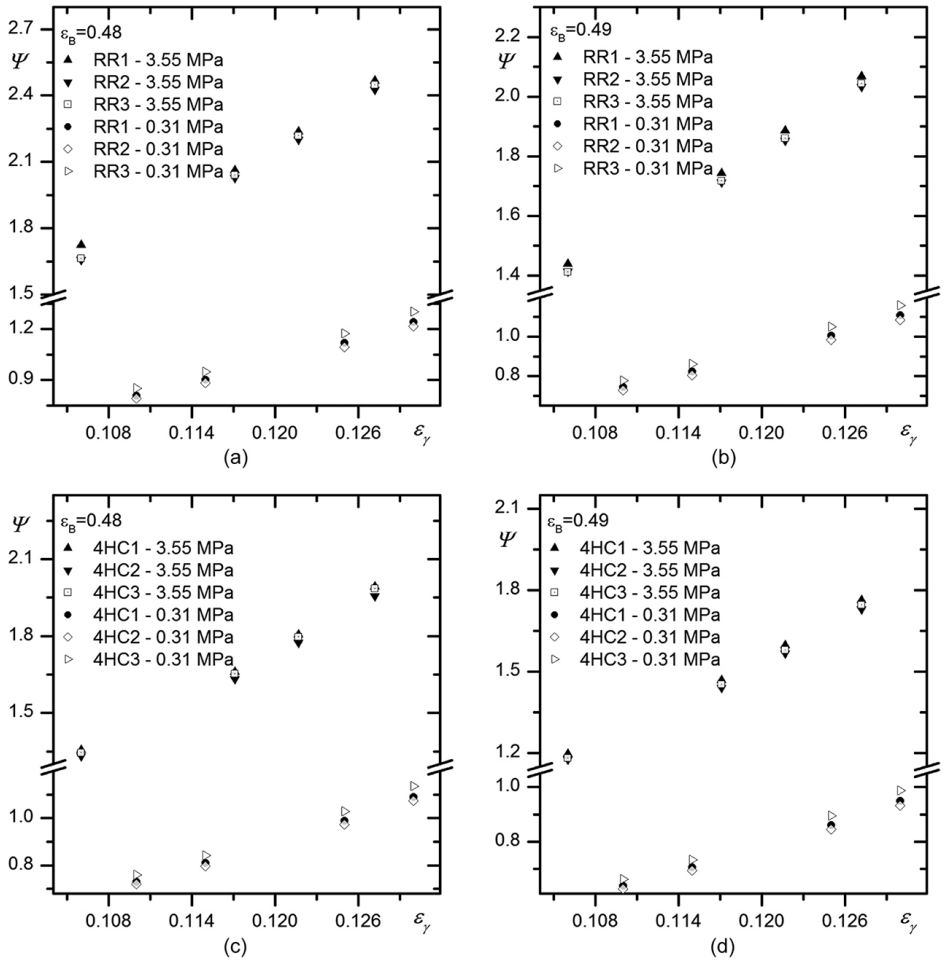

Figure 6: (a) Dimensionless pressure drop in a bed of RR with bed porosity of 0.48, using IMEMs S1, S4 and S7 at different liquid holdups, (b) at different liquid holdups in a bed of RR with bed porosity of 0.49, using IMEMs S1, S4 and S7 at different liquid holdups. (c) Dimensionless pressure drop in a bed of 4HC with bed porosity of 0.48, using IMEMs S1, S4 and S7 at different liquid holdups. (d) Dimensionless pressure drop in a bed of 4HC with bed porosity of 0.49, using IMEMs S1, S4 and S7 at different liquid holdups.

Regarding to the bed porosity effect, the pressure drop obtained for bed porosity of 0.48 are 68.1 %, and 19.94 % higher than for bed porosity of 0.49 for RR particles at high and low operation pressure respectively. For 4HC particles, the variation from bed porosity of 0.48 to 0.49, are 39.66 % and 23.58 % higher at high and low operation pressure respectively.

It is important to note that the models of other geometries rather than spheres were constructed with the same porosity, so that differences in the pressure drop cannot be attributed to the different porosity produced by different shapes, as this is not the case of these simulations. An indicator of what could cause differences in the values of pressure drop can be seen in Figure 7, where there are significant differences in the distribution and flow velocity due to differences in interstitial space within the beds.

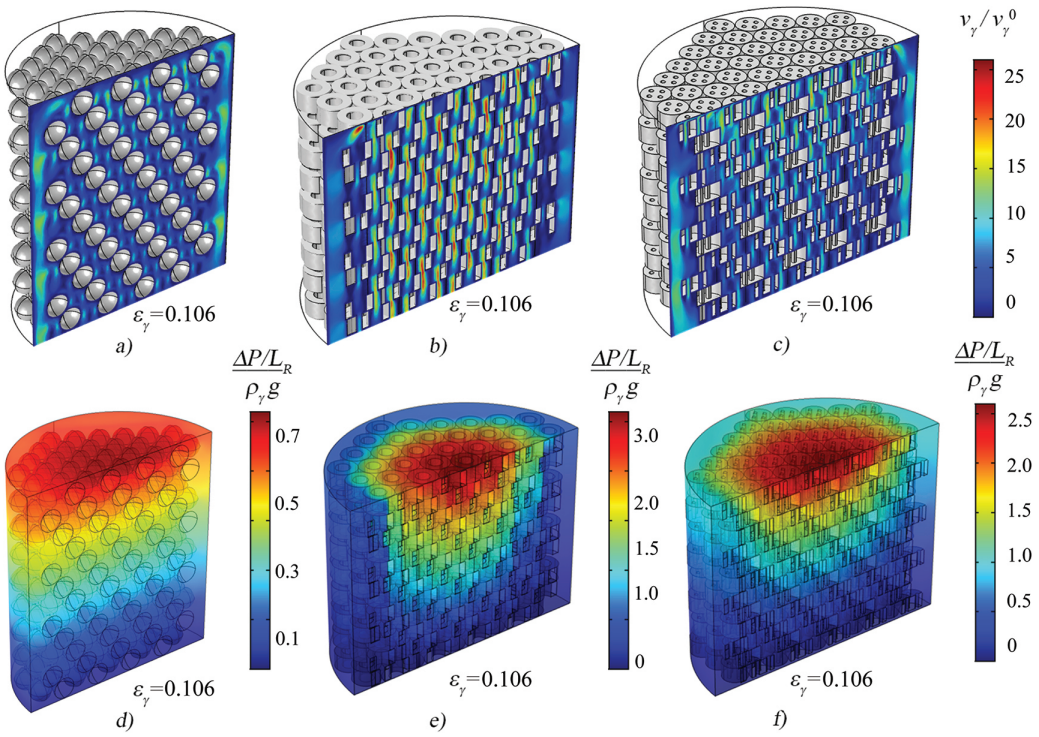

Figure 7: Comparison of dimensionless velocity field for (a) spheres (b) RR (c) 4HC, and dimensionless pressure drop for (d) spheres (e) RR (f) 4HC with IMEM 1 and bed porosity of 0.48.

Figure 7(a), Figure 7(b) and Figure 7(c) show the dimensionless interstitial velocity for the three geometries considered in this study. As it can be seen, an important effect of variation of porosity across reactor radius over liquid velocity field which is also associated to wall effects in a zone that represents less of 10 %; also, it can be seen that the bed with spheres lead to a more uniform distribution of liquid velocities and less channeling; on the opposite extreme, the bed with 4HC shows higher non homogeneities and variations in the velocity fields, leading to higher pressure drops. The aforementioned implies that the fluid in the bed with spherical particles uses almost all interstitial space to flow, the restriction to flow within the bed is slightly variable, and thus the distribution of fluid and its velocity is more uniform; while in the case of beds with RR and 4HC, the geometrical characteristics of the pellets lead to zones in the bed with high variable restrictions to flow, leading to liquid maldistribution with zones with higher channeling and/or bypassing and zones of stagnant fluid within the bed.

As catalyst shapes were constructed with equal S_T/V_P ratio for all pellets, then, the difference in pressure drop observed in Figure 5, Figure 6 and Figure 7, cannot be attributed to differences in porosity, or to a different flow cross-sectional area caused by the shape of the pellet. Actually, the main changes are evidently the distribution and geometry of the flow areas, and the amount of fluid-solid interfacial area $\left(\mathrm{A}_{f\omega}\right)$; which values are 0.002604, 0.005084 and 0.01199 m^2 for spheres, 4HC and RR particles respectively, implying that the bed packed with 4HC catalyst has almost double of fluid-solid interfacial area than the spheres and more than three and a half times more for the case of RR. Hence the difference in pressure drop can be attributed to bed textural aspects (tortuosity, restriction factors and differences in superficial area).

On another hand, it is recognized in the literature the presence of wall effects associated with the variation of porosity. In this sense, it is possible to find a great diversity of values suggested for the necessary values of N to discard these effects, varying between 3 or 4 to more than 100 particle diameters. In relation to this, in Figure 7(a) Figure 7(b) and Figure 7(c) it can be seen that in the regions near the reactor walls, the fluid exhibits channeling. For the selection of $N \approx 9.1$ in the hydrodynamics model, these wall effects are not present in a zone that represents between 83 % and 89 % of the total bed; while in the coupled model, considering $N \approx 18.4$, the zone free of wall effects hydrodynamics of TBR is between 91.7 % and 94.4 %.

In summary, it can be observed in a zone with length of 1 to 1.5 pellet diameters, which is consistent with the remarks of Doari et al., and Giese et al. over wall effects over hydrodynamics (Dorai et al. 2015; Giese, Rottschäfer, and Vortmeyer 1998), who point out that the region where bypass flow is presented in a region of a typical width of 2–3 pellet diameters. The analysis of the effect of the proximity of the reactor walls on velocity, concentration and their fluxes fields, for the species considered in the model (see Figure 7 and Figure 8), suggest that the region where wall effects are significant represents about 5 % of the total velocity and con-

centration fields; so, it can be assumed that this N value provides representative values in the velocity ($N \simeq 9.1$) and concentration fields ($N \simeq 18.4$) in ours CFD simulation, although simulations with $N > 20$ are desirable.

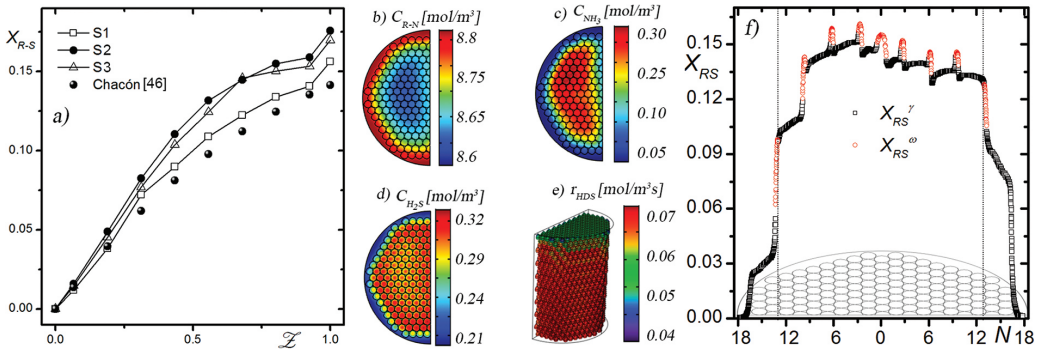

Figure 8: (a) Average HDS conversion along dimensionless reactor length using the IMEMs with the best prediction for hydrodynamics analysis, against literature data. (b–e) Concentration field for both liquid and solid domain in a cut plane at middle of reactor length for: (b) nitrated species, (c) ammonia, (d) hydrogen sulfide, and (e) predicted HDS reaction rate values at pellet domain. (f) HDS conversion in a cut line along the reactor diameter for both liquid and solid domain in a cut plane at middle of reactor length.

Since the analysis of wall effects was first performed on the hydrodynamic model and then on the hydrodynamic model that couples the mass transport, the observations suggest that the value of N depends strongly on the system analyzed, that is, on whether the system is a cold column (without reaction) or if the system includes reaction, and possibly depends of another aspects like how so fast is the reaction, whether it is exothermic or endothermic, and even on geometric aspects and pellet and reactor dimensions; so that a unique value of N valid to all possible system of interest is very unviable and it could represent great uncertainty.

Figure 8(a) shows the conversion for HDS reaction obtained using three different IMEM's against data from literature (Chacón et al. 2012). As can be seen, the effect of the IMEM over the predicted conversion values is more pronounced than on the hydrodynamic parameters such as dimensionless pressure drop (see Figure 5(a) and Figure 5(b), with differences of 17.9 % and 14 % for S2 y S3 and using as reference the S1 model. Figure 8(b), Figure 8(c), Figure 8(d) and Figure 8(e) show the distribution of nitrated $(R-N)$ species, ammonia(NH_3), hydrogen sulfide (H_2S) concentrations in both liquid and solid phases in a radial cut plane at the middle reactor length, and reaction rate for HDS reaction. In Figure 8(b) and Figure 8(c), a pronounced wall effect can be observed over concentrations in a region of about 2 particle diameters away from the reactor wall (representing $\sim$ 10% for a system with $N \approx 18.4$), this effect is most evident in Figure 8(f) where is observed an abrupt change in the behavior of HDS conversion in a region of size of about 2 particle diameters away from the reactor wall. Similar behavior takes place in the diffusive fluxes regarding to wall effects.

Regarding the sulfurized specie conversion, it is noteworthy that Chacon's model was solved for a reactor of 12 cm in length, obtaining 80 % in exit conversion, and had a conversion of 14.1 % at 7 mm in reactor length, the conversion achieved in simulations of the 7 mm model is very close to that reported by Chacon (Chacón et al. 2012) with a MARE of 5.12 %. Hence, the model presented here couples the hydrodynamics and mass transport with heterogeneous reaction, and provides good estimates for both hydrodynamics parameters and HDS conversion.

The model also has the potential of reviewing in detail information from other theoretical and experimental work that is inaccessible. In this context, a deeper understanding and analysis of kinetic behavior of the model HDS reactor, considering different operating conditions, the possible effects on the size and geometry of the catalyst and the porosity of the catalyst bed is desirable, however, this will be the scope of another complementary publication.

4 Conclusions

It was implemented a three-phase CFD simulation of a HDS reactor to desulfurize light gasoil that operates in trickle regime, and where the hydrodynamics of two fluid phases was coupled with mass transport within the fluid and the catalyst phase. The effect of geometry of catalytic bed because of variations of the bed porosity and catalyst geometry over the hydrodynamic behavior of the reactor and in particular on the prediction of the pressure drop was analyzed. The model was validated against experimental data comparing pressure drop at both, low and high operation pressures, and against theoretical conversion data found in literature, obtaining

excellent predictions of hydrodynamic parameters, with 5 times better accuracy in predicting pressure drops, and 50 % improvement in holdup prediction.

It can be concluded that the excellent accuracy in pressure drop prediction is due to the coupling of 1) a suitable IMEM; 2) incorporating essential geometrical detail of interstitial spaces of the catalytic bed and its variations, like the a distribution of the flow areas, differences in interfacial particle areas and tortuosity inherent to pellet shape; and 3) a correct form to compare two TBR's with different length scales (a suitable scaling-up procedure) that allow to obtain similar values for the key hydrodynamics parameters as ΔP and ε_γ, and similar values for the predicted conversion XHDS. In addition, our results suggest that equaling ε_γ–ε_β or L-G lead to similar hydrodynamic and kinetic predictions between two reactors of different length scale. These results could mean a finding that eventually allows the establishment of scaling techniques based on a more scientific basis.

The present document presents an analysis of the TBR scaling process; however, its results are not conclusive, as it is yet desirable to analyze and compare several reactors of different dimensions and involving different processes.

Regarding to the validity of the gas-solid momentum exchange Attou's closure term as used here, the results suggest that IMEM S1 is adequate to model the TBR hydrodynamics at low and high-pressure operation; moreover, when coupling hydrodynamics with mass transport/reaction, S1 model seems to be the most successful yet. In addition, the results show that the use of other gas-solid momentum exchange models that imply stronger interaction between gas and solid phases are not necessary.

It is important to remark that the implemented CFD model incorporates the mass transport of H_2, H_2S, NH_3, nitrated (R-N) and sulfurated species (R-S) between two fluid phases and a solid phase with simultaneous HDS and HDN reaction, which take place inside the catalyst domain. In addition, also couples the mass transport with the two liquid phases' hydrodynamic. The complete model implies 13 mass transport equations per species, two momentum transport equations for fluid phases, and three closures for the interactions between phases (IMEM's). This level of detail allows to study phenomenological aspects of TBR's that are inaccessible to most of the models found in literature, for example the analysis of N values performed in this work, for which the concentration/flux fields details for several species were used. This model can be used to extent the analysis considering different operation conditions, catalyst shapes, other parallel reactions, etc.

Finally, it should be noted that an analysis of the wall effects was performed and it was found that a value of $N \simeq 9.1$ for Hydrodynamics model and other of $N \simeq 18.4$ for hydrodynamics coupled with mass transport for HDS system are adequate to consider that wall effects can be neglected. Then it can be concluded, that the possibility of establishing a single value is remote. A particular result of our study, is that the magnitude of the appropriate N value, must be determined specifically by characteristics of the problem studied.

Nomenclature

Symbols		
a_S	$[m^{-1}]$	Pellet specific area
a_v	$[m^{-1}]$	Catalyst microstructure specific area
A_T	$[m^2]$	Transversal area of the reactor
API		API gravity of gasoil
$A_{j\omega}$	$[m^2]$	Solid-fluid interphase
C_D		Drag coefficient
C_i^j	$[mol\ m^3]$	Concentration of specie i in i-phase
$\langle C_i^\omega \rangle^\omega$	$[mol\ m^3]$	Average concentration of specie i in solid pseudo ω
d_b	[mm]	Bubble diameter
D_i^j	$[m^2 s^{-1}]$	Effective diffusivity of specie i in $j$phase
D_i^j	$[m^2 s^{-1}]$	Diffusivity of specie i in j-phase
$\mathbf{D}_{eff,i}^\omega$	$[m^2 s^{-1}]$	Effective diffusivity of specie i in pellet domain
d_h	[m]	Hydraulic diameter
d_p	[m]	Pellet diameter
D_R	[m]	Reactor diameter
ΔH_{HDS}	$[J\ mol^{-1}]$	Heat of reaction
$E_{a,j}$	$[J\ mol^{-1}]$	j reaction activation energy
E_1		First Ergun constant
E_2		Second Ergun constant
F_i	$[N\ m^{-3}][N\ m^{-3}]$	Interaction force term

g	$[\mathrm{m\ s^{-2}}]$	Gravitational constant
G	$[\mathrm{kg\ m^{-2}s^{-1}}]$	Gas mass flow
Ga_γ		Galilei number
H_i	$[\mathrm{m^3Pa\ mol^{-1}}]$	Henry coefficient for specie i
k_{HDS}	$\left[\left(\frac{\mathrm{m^3}}{\mathrm{mol}}\right)^{0.5}\mathrm{s^{-1}}\right]$	Pre-exponential factor for HDS reaction
k_{HDS}	$[\mathrm{m^3mol^{-1}}s^{-1}]$	Pre-exponential factor for HDN reaction
k_i^0	$[\mathrm{m^3\ mol^{-1}}]$	Pre-exponential factor for adsorption of i specie
K_i	$[\mathrm{mol\ m^{-3}}]$	Specie i adsorption constant
$K_{g,i}^{\beta\gamma}$	$[\mathrm{s^{-1}}]$	Gas-liquid mass transfer coefficient for specie i
$K_i^{\gamma\omega}$	$[\mathrm{m\ s^{-1}}]$	Liquid-solid mass transfer coefficient for specie i
K_{ji}	$[\mathrm{kg\ m^{-3}s^{-1}}]$	Momentum exchange coefficient between i and j phases
L	$[\mathrm{kg\ m^{-2}s^{-1}}]$	Liquid mass flow
L_R	[m]	Reactor length
l_P	[m]	Solid particle length
MW	$[\mathrm{g\ mol^{-1}}][\mathrm{g\ mol^{-1}}]$	Gasoil molecular weight
$N_i^{\beta\gamma}$	$[\mathrm{mol\ m^{-3}s^{-1}}]$	Volumetric mass exchange of specie i between gas and liquid phases
$\mathbf{N}_i^j$	$[\mathrm{kg\ m^{-2}s^{-1}}]$	Total mass flux of specie i
$-\mathbf{n}$		Unitary normal vector
N		Reactor to pellet diameter ratio
N_c		Critical reactor to pellet diameter ratio
P	[Pa]	Total pressure
Q_i	$[\mathrm{J\ mol^{-1}}]$	Specie i adsorption energy
$\langle r^\omega \rangle^\omega$	$[\mathrm{mol\ m^{-3}s^{-1}}]$	Average reaction rate
r_P	[m]	Pellet radius
r_R	[m]	Reactor radius
R_g	$[\mathrm{J\ mol^{-1}K}]$	Constant of ideal gases
Re^i		Reynolds number for phase i
S_T	$[\mathrm{m^2}]$	Cross-sectional area
T_i	[K]	i phase temperature
V_P	$[\mathrm{m^3}]$	Volume of the solid particle
V_i	$[\mathrm{m^3\ mol^{-1}}]$	Molar volume of specie i
$V_{N,i}$	$[\mathrm{m^3\ mol^{-1}}]$	Molar volume of specie i at standard conditions
$\mathbf{v}_i$	$[\mathrm{m\ s^{-1}}]$	i phase local interstitial velocity
$(\mathbf{v}_j - \mathbf{v}_i)$	$[\mathrm{m\ s^{-1}}]$	slip velocity between j and i phases
v_i^0	$[\mathrm{m\ s^{-1}}]$	i phase inlet velocity
We_γ		Weber number
X_i		Specie i conversion
X_β		Lockhart-Martinelli parameter

Greek symbols

β		Gas phase
γ		Liquid phase
ω		Solid pseudophase
ε_i		i phase volume fraction
ε_γ		Liquid holdup
ε_σ		Pellet porosity
ε_B		Bed porosity
μ_i	[Pa s]	Specie i dynamic viscosity
ρ_i	$[\mathrm{kg\ m^{-3}}]$	Specie i density
ρ_{20}	$[\mathrm{kg\ m^{-3}}]$	Gasoil density at 20 °C
σ_γ	[N m]	Liquid surface tension
π		Pi number
ν_i		Specie i stochiometric coefficient
λ_i		Specie i solubility
Ψ		Dimensionless pressure drop

Sub- and Superscripts

0		Initial conditions
op		Operation conditions

Abbreviations

GHSV	$[\mathrm{s^{-1}}]$	Gas hourly space velocity
LHSV	$[\mathrm{s^{-1}}]$	Liquid hourly space velocity
MARE		Mean absolute relative error
IMEM		Interphase momentum exchange model

CFD	Computational Fluid Dynamics
TBR	Trickle Bed Reactor
TBRs	Trickle Bed Reactors
TBR's	That belong to the trickle Bed Reactor
4HC	Cylinders with four longitudinal holes
RR	Raschig rings
EXP	Experimental value
CALC	Calculated value with CFD model
HDS	Hydrodesulphurization
HDN	Hydrodenitrogenation
$R-S$	Sulfurized specie
$R-N$	Nitrated specie
H_2S	Hydrogen sulfide
NH_3	Ammonia
N_2	Nitrogen
H_2	Hydrogen

References

Afandizadeh, S., and E. A. Foumeny. 2001. "Design of Packed Bed Reactors: Guides to Catalyst Shape, Size, and Loading Selection." *Applied Thermal Engineering* 21:669–682.

Ahmed, T. *Hydrocarbon Phase Behavior*. Houston: Ed. Gulf Publishing Company, 1989.

Al-Dahhan, M. H., and M. P. Dudukovic. 1994. "Pressure Drop and Liquid Holdup in High Pressure Trickle-Bed Reactors." *Chemical Engineering Sciences* 49:5681–5698.

Al-Dahhan, M. H., and M. P. Dudukovic. 1995. "Catalyst Wetting Efficiency in Trickle-Bed Reactors at High Pressure." *Chemical Engineering Sciences* 50:2377–2389.

Anderson, T. B., and R. Jackson. 1967. "Fluid Mechanical Description of Fluidized Beds. Equations of Motion." *Industrial & Engineering Chemical Fundamentals* 6:527–539.

Atta, A., S. Roy, and K. D. P. Nigam. 2007. "Prediction of Pressure Drop and Liquid Holdup in Trickle Bed Reactor Using Relative Permeability Concept in CFD." *Chemical Engineering Sciences* 62:5870–5879.

Atta, A., R. Shantanu, and K. D. P. Nigam. 2009. "CFD Prediction of Hydrodynamics in High-Pressure Trickle Bed Reactor." *Journal Chemical Engineering Japanese* 42:119–124.

Attou, A., C. Boyer, and G. Ferschneider. 1999. "Modelling of the Hydrodynamics of the Cocurrent Gas–Liquid Trickle Flow through a Trickle-Bed Reactor." *Chemical Engineering Sciences* 54:785–802.

Augier, F., F. Idoux, and J. Y. Delenne. 2010. "Numerical Simulation of Transfer and Transport Properties inside Packed Beds of Spherical Particles." *Chemical Engineering Sciences* 65:1055–1064.

Augier, F., A. Koudil, A. Royon-Lebeaud, L. Muszynski, and Q. Yanouri. 2010. "Numerical Approach to Predict Wetting and Catalyst Efficiencies inside Trickle Bed Reactors." *Chemical Engineering Sciences* 65:255–260.

Auset, M., and A. A. Keller. 2004. "Pore-Scale Processes that Control Dispersion of Colloids in Saturated Porous Media." *Water Resources Researcher* 40:1–11.

Bandari, M., Y. Behjat, and S. Shahhosseini. 2012. "CFD Investigation of Hydrodynamic and Heat Transfer Phenomena around Trilobe Particles in Hydrocracking Reactor." *International Journal of Chemical Reactions Engineering* 10:1–19.

Bazmi, M., S. H. Hashemabadi, and M. Bayat. 2012. "CFD Simulation and Experimental Study of Liquid Flow Mal-Distribution through the Randomly Trickle Bed Reactors." *International Communicable in Heat Massachusetts* 29:736–743.

Bazmi, M., S. H. Hashemabadi, and M. Bayat. 2013. "Development of a Pellet Scale Model for Trickle Bed Reactor Using CFD Techniques." *Journal of Petroleum Science and Technology* 3:21–30.

Beni, A. H., and M. R. Khosravi-Nikou. 2016. "Modeling Hydrodynamics of Trickle-Bed Reactors at High and Low Pressure Using CFD Method." *Journal of Petroleum Science and Technology* 3:1770–1779.

Botchwey, C., A. K. Dalai, and J. Adjaye. 2003. "Product Selectivity during Hydrotreating and Mild Hydrocracking of Bitumen-Derived Gas-Oil." *Energy & Fuels* 17:1372–1381.

Carbonell, R. G. 2000. "Multiphase Flow Models in Packed Beds." *Oil & Gas Science and Technology* 55:417–425.

Carruthers, J. D., and D. J. DiCamillo. 1988. "Pilot Plant Testing of Hydrotreating Catalyst: Influence of Catalyst Condition, Bed Loading and Dilution." *Applied Catalysis* 43:253–276.

Chacón, R., A. Canale, A. Bouza, and Y. Sanchez. 2012. "Modelling of a Three-Phase Reactor for Bitumen-Derived Gas Oil Hydrotreating." *Brazilian Journal Chemical Engineering* 29:135–146.

Chrust, M., S. Goujon-Durand, and J. E. Wesfried. 2013. "Loss of a Fixed Plane of Symmetry in the Wake of a Sphere." *Journal of Fluids and Structures* 41:51–56.

Cordero, M. E., R. Natividad, L. G. Zárate, J. A. Hernandez-Servin, and J. Salas. 2014. "Estimation of Effective Diffusion Coefficient and Its Effect on Effectiveness Factor for HDS Catalytic Process: A Multi-Scale Approach." *Catalysis Today* 220-222:113–123.

Derkx, O. R., and A. G. Dixon. 1996. "Determination of the Fixed Bed Wall Heat Transfer Coefficient Using Computational Fluid Dynamics." *Numerical Heat Transfer, Part A Applications* 29:777–794.

Dorai, F., C. M. Teixeria, M. Rolland, E. Climent, M. Marcoux, and A. Wachs. 2015. "Fully Resolved Simulations of the Flow through a Packed Bed of Cylinders: Effect of Size Distribution." *Chemical Engineering Sciences* 129:180–192.

Drew, D. A. 1983. "Mathematical Modeling of Two-Phase Flow." *Annals Reviews Fluid Mechanisms* 15:261–291.

Dudukovic, M. P. 2007. "Relevance of Multiphase Reaction Engineering to Modern Technological Challenges." *Industrial Engineering Chemical Researcher* 46:8674–8686.
Dudukovic, M. P. 2009. "Challenges and Innovations in Reaction Engineering." *Chemical Engineering Commission* 196:252–266.
Ellman, M. J., N. Midoux, G. Wild, and J. Charpentier. 1990. "A New, Improved Liquid Hold-Up Correlation for Trickle-Bed Reactors." *Chemical Engineering Sciences* 45:1677–1684.
Froment, G., F, and K. B. Bischoff. *Chemical Reactor Analysis and Design*. New York: Wiley, 1979.
García-Martínez, J., A. Dutta, G. Chávez, J. A. De Los Reyes, and C. O. Castillo-Araiza. 2015. "Hydrodesulfurization of Dibenzothiophene in a Micro Tricke Bed Catalytic Reactor under Operating Conditions from Reactive Distillation." *International Journal Chemical Reactions Engineering* 10:769–783.
Gianetto, A., and V. Specchia. 1992. "Trickle-Bed Reactors: State of Art and Perspectives." *Chemical Engineering Sciences* 47:3197–3213.
Gidaspow, D. *Multiphase Flow and Fluidization: Continuum and Kinetic Theory Descriptions*. Boston: Academic Press, 1994.
Giese, M., K. Rottschäfer, and D. Vortmeyer. 1998. "Measured and Modeled Superficial Flow Profiles in Packed Beds with Liquid Flow." *AIChE Journal* 44:484–490.
Goto, S., and J. M. Smith. 1975. "Trickle-Bed Reactor Performance. Part I. Holdup and Mass Transfer Effects." *AIChE Journal* 21:706–713.
Guardo, A., M. Coussirat, F. Recasens, M. A. Larrayoz, and X. Escaler. 2006. "CFD Study on Particle-To-Fluid Heat Transfer in Fixed Bed Reactors: Convective Heat Transfer at Low and High Pressure." *Chemical Engineering Sciences* 6:4341–4353.
Gujal, P. R., V. V. Ranade, and R. V. Chaudhari. 2005. "Computational Study of a Single-Phase Flow in Packed Beds of Spheres." *AIChE Journal* 51:365–378.
Gunjal, P., and V. V. Ranade. 2007. "Modelling of Laboratory and Commercial Scale Hydro-Processing Reactors Using CFD." *Chemical Engineering Sciences* 66:5512–5526.
Holub, R. A., M. P. Dudukovic, and P. A. Ramachandran. 1992. "A Phenomenal Model for Pressure Drop, Liquid Holdup, and Flow Regime Transition in Gas-Liquid Trickle Flow." *Chemical Engineering Sciences* 47:2343–2348.
Horgue, P., F. Augier, P. Duru, M. Prat, and M. Quintard. 2013. "Experimental and Numerical Study of Two-Phase Flows in Arrays of Cylinders." *Chemical Engineering Sciences* 102:335–345.
Hu, G., and D. Li. 2007. "Multiscale Phenomena in Microfluidics and Nanofluidics." *Chemical Engineering Sciences* 62:3443–3454.
Iliuta, I., and F. Larachi. 1999. "The Generalized Slit Model: Pressure Gradient, Liquid Holdup & Wetting Efficiency in Gas–Liquid Trickle Flow." *Chemical Engineering Sciences* 45:5039–5045.
Iliuta, I., F. Larachi, and B. P. A. Grandjean. 1988. "Pressure Drop and Liquid Holdup in Trickle Flow Reactors: Improved Ergun Constants and Slip Correlations for the Slit Model." *Industrial Engineering Chemical Researcher* 37:4542–4550.
Ishii, M. *Thermo-Fluid Dynamic Theory of Two Phase Flow*. Paris: Eyrolles, 1975.
Jindal, A., and V. V. Buwa. 2016. "Effect of Bed Characteristics on Local Liquid Spreading in a Trickle Bed." *AIChE Journal* 63:347–357.
Katz, D. L., Cornell D, Kobayashi R, F. H. Poettmann, J. A. Vary, J. R. Elenbaas, and C. F. Weinaug. *Handbook of Natural Gas Engineering*. New York: McGraw-Hill, 1959.
Kundu, A., K. D. P. Nigam, and R. P. Verma. 2003. "Catalyst Wetting Characteristics in Trickle-Bed Reactors." *AIChE Journal* 49:2253–2263.
Lappalainen, K., M. Manninen, and V. Alopaeus. 2009. "CFD Modeling of Radial Spreading of Flow in Trickle-Bed Reactors Due to Mechanical and Capillary Dispersion." *Chemical Engineering Sciences* 64:207–218.
Larachi, F., A. Laurent, N. Midoux, and G. Wild. 1991. "Experimental Study of a Trickle-Bed Reactor Operating at High Pressure: Two-Phase Pressure Drop and Liquid Saturation." *Chemical Engineering Sciences* 46:1233–1246.
Lasseux, D., and F. J. T. Valdés-Parada. 2017. "Symmetry Properties of Macroscopic Transport Coefficients in Porous Media." *Physical Fluid* 29:043303–1–19.
Liu, G., J. Lan, Y. Cao, Z. Huang, Z. Cheng, and Z. Mi. 2009. "New Insights into Transient Behaviors of Local Liquid-Holdup in Periodically Operated Trickle-Bed Reactors Using Electrical Capacitance Tomography (ECT)." *Chemical Engineering Sciences* 64:3329–3343.
Lopes, R. J. G., and R. M. Quinta-Ferreira. 2009. "Turbulence Modelling of Multiphase Flow in High-Pressure Trickle-Bed Reactors." *Chemical Engineering Sciences* 64:1806–1819.
Lopes, R. J. G., and R. M. Quinta-Ferreira. 2010a. "Evaluation of Multiphase CFD Models in Gas–Liquid Packed-Bed Reactors for Water Pollution Abatement." *Chemical Engineering Sciences* 65:291–297.
Lopes, R. J. G., and R. M. Quinta-Ferreira. 2010b. "Assessment of CFD Euler–Euler Method for Trickle-Bed Reactor Modelling in the Catalytic Wet Oxidation of Phenolic Wastewaters." *Chemical Engineering Sciences* 160:293–301.
Lugo-Méndez, H. D., F. J. Valdés-Parada, M. L. Porter, B. D. Wood, and A. O. Ochoa-Tapia. 2015. "Upscaling Diffusion and Nonlinear Reactive Mass Transport in Homogeneous Porous Media." *Transport in Porous Media* 107:683–716.
Macias, M., and J. Ancheyta. 2004. "Simulation of an Isothermal Hydrodesulfurization Small Reactor with Different Catalyst Particle Shapes." *Catalysis Today* 98:243–252.
Malang, J., P. Kumar, and A. Saptoro. 2015. "Computational Fluid Dynamics-Based Hydrodynamics Studies in Packed Bed Columns: Current Status and Future Directions." *International Journal Chemical Reactions Engineering* 13:289–303.
Mederos, F. S., and J. Ancheyta. 2007. "Mathematical Modeling and Simulation of Hydrotreating Reactors: Cocurrent versus Countercurrent Operations." *Applied Catalysis A: General* 332:8–21.
Mital, R. 1998. "Planar Symmetry in the Unsteady Wake of a Sphere." *AIAA Journal* 37:388–390.
Mitra, S. *Computational Dynamics Modeling of Trickle Bed Reactors- Hydrodynamics, Reactor Internals, Catalyst Bed*. USA: VM. Verlag Dr Müller, 2011.
Mousazadeh, F., H. E. A. Van Den Akker, and R. F. Mudde. 2013. "Direct Numerical Simulation of an Exothermic Gas-Phase Reaction in a Packed Bed with Random Particle Distribution." *Chemical Engineering Sciences* 100:259–265.
Nadeem, H., I. B. Salem, and M. Sassi. 2017. "Experimental Visualization and Investigation of Multiphase Flow Regime Transitions in Two-Dimensional Trickle Bed Reactors." *Chemical Engineering Commission* 204:388–397.
Nemec, D., and J. Levec. 2005. "Flow Trhough Packed Bed Reactors: 2. Two-Phase Concurret Downflow." *Chemical Engineering Sciences* 60:6958–6970.

Niegodajew, P., D. Asendrych, and S. Drobniak. 2013. "Numerical Modelling of CO_2 Desorption Process Coupled with Phase Transformation and Heat Transfer in CCS Installation." *Journal of Power Technologies* 93:354–362.

Nijemeisland, M., and A. G. Dixon. 2001. "Comparison of CFD Simulations to Experiment for Convective Heat Transfer in a Gas-Solid Fixed Bed." *Chemical Engineering Journal* 82:231–246.

Partopour, B., and A. G. Dixon. 2016. "Reduced Microkinetics Model for CFD Simulation of the Fixed Bed Partial Oxidation of Ethylene." *Industrial Engineering Chemical Researcher* 55:7296–7306.

Peng, W., M. Xu, X. Huai, and Z. Liu. 2016. "3D CFD Simulations of Acetone Hydrogenation in Randomly Packed Beds for an Isopropanol–Acetone–Hydrogen Chemical Heat Pump." *Applied Thermal Engineering* 94:238–248.

Prasad, V., A. M. Karim, Z. Ulissi, M. Zagrobelny, and D. G. Vlachos. 2010. "High Throughput Multiscale Modeling for Design of Experiments, Catalysts, and Reactors: Application to Hydrogen Production from Ammonia." *Chemical Engineering Sciences* 65:240–246.

Raynal, L., F. Augier, F. Bazer-Bachi, Y. Haroun, and C. Pereira Da Fonte. 2015. "CFD Applied to Process Development in the Oil and Gas Industry – A Review." *Oil & Gas Science and Technology Review* 71:1–24.

Reddy, R. K., and J. B. Joshi. 2010. "CFD Modeling of Pressure Drop and Drag Coefficient in Fixed Beds: Wall Effects." *Particuology* 8:37–43.

Sie, S. T. 1990. "Scale Effects in Laboratory and Pilot-Plant Reactors for Trickle-Flow Processes." *Revue de l'Institut français du pétrole* 46:501–515.

Solomenko, Z., Y. Haroun, M. Fourati, F. Larachi, C. Boyer, and F. Augier. 2015. "Liquid Spreading in Trickle-Bed Reactors: Experiments and Numerical Simulations Using Eulerian-Eulerian Two-Fluid Apphoach." *Chemical Engineering Sciences* 126:698–710.

Speccia, V., G. Baldi, and A. Gianetto. 1978. "Solid-Liquid Mass Transfer in Concurrent Two-Phase Flow through Packed Beds." *Industrial Engineering Chemical Proceedings Design Developments* 17:362–367.

Trivizadakis, M. E., D. Giakoumakis, and A. J. Karabelas. 2006. "A Study of Particle Shape and Size Efect on Hydrodynamics Parameters of Trickle Beds." *Chemical Engineering Sciences* 61:5534–5543.

Wei, D., Z. Jianzhou, L. Panpan, X. Jian, W. Weisheng, H. Guangxiang, and Z. Lifeng. 2017. "Advanced Understanding of Local Wetting Behaviour in Gas-Liquid-Solid Packed Beds Using CFD with a Volume of Fluid (VOF) Method." *Chemical Engineering Sciences* 36:3292–3314.

Wen, C. Y., and Y. H. Yu. 1966. "Mechanics of Fluidization." *Chemical Engineering Progress Symposium Series* 62:100.

Whitaker, S. *The Method of Volume Averaging*. Netherlands: Kluwer Academic Publishers, 1999.